published by Ural Federal University
eISSN 2411-1414
chimicatechnoacta.ru

REVIEW
2023, vol. 10(2), No. 202310203
DOI: 10.15826/chimtech.2023.10.2.03

Application of the similarity theory to analysis of photocatalytic hydrogen production and photocurrent generation

Dina V. Markovskaya *, Ekaterina A. Kozlova

Department of heterogeneous catalysis, Boreskov Institute of Catalysis, Novosibirsk 630090, Russia
* Corresponding author: madiva@catalysis.ru

This paper belongs to a Regular Issue.

Abstract

In this research some methods of the similarity theory were quantitatively applied to the description of the relationship between the efficiencies of the photocatalytic hydrogen production and photocurrent generation for the first time. Two possible similarity criteria, namely, such as the ratio of the number of electrons involved in the photocatalytic reaction to the generation of photocurrent ones and the ratio of energies transformed in the case of photocatalytic hydrogen evolution to the photocurrent, were obtained by the dimensional analysis. The literature data allow checking the first criterion. The application of the first possible similarity criterion to the samples with different chemical nature, solid solutions, series, in which the synthesis time or the ratio of catalyst components, electrolyte amount or its nature is changed, was analyzed. It was shown that the ratio of electrons may serve as the similarity criterion only under the conditions of geometric and physical similarities.

Keywords

photocatalysis
hydrogen evolution
photocurrent generation
theory of similarity
similarity criterion
dimension theory

Received: 13.02.23
Revised: 20.03.23
Accepted: 26.03.23
Available online: 04.04.23

Key findings

- Photocatalytic hydrogen production and photocurrent generation are the analogous phenomena.
- Two possible similarity criteria were proposed.
- Ratio of the electron numbers acts as a similarity criterion if the conditions of geometric and physical similarity are fulfilled.

1. Introduction

Nowadays different processes and phenomena whose realization allows generating energy are of particular importance. The traditional method of burning fuel resources has a significant disadvantage associated with the limited reserves of the corresponding resources. Accordingly, the search for alternative fuels is known to be an urgent task of modern science [1]. Since the 70s, the idea of using hydrogen as a fuel has gained particular popularity among researchers [1, 2]. Hydrogen is known to be one of the most common elements on Earth and can be obtained from various compounds. When hydrogen is burned, eco-friendly water is formed, and the large amount of heat is realized. However, in this case the question arises about new methods of hydrogen synthesis, because the main methods either use non-renewable energy sources or are quite energy intensive [1]. One of the promising alternative ways to produce hydrogen is the photocatalytic method, implemented in the presence of photocatalysts based on semiconductors. An important feature of this method is the use of sunlight. Thus, in fact, we are talking about the conversion of light energy into the energy of chemical bonds occurring on the semiconductor surface [3].

It should be noted that the energy from light can be generated in the photoelectrochemical cells. These processes are often carried out on electrodes made of semiconductors. It is noteworthy that in the case of photocatalytic hydrogen production and photocurrent generation, the same physicochemical processes such as the formation of exciton, the formation of an electron-hole pair, the spatial separation of charge carriers during their migration to the boundaries of the phase interface, interphase transfer to the components of the reaction medium occur on the semiconductor surface

[4–7]. The main difference lies only in the fact that in the case of photoelectrochemical cells, besides participating in various transformations, electrons are transferred to counter electrodes, and for photocatalytic hydrogen evolution, the reaction occurs directly on the surface of semiconductor particles [7]. The similarity of the principles of functioning of these two phenomena can be useful in the development of various strategies for improving the target characteristics of materials. It should be noted that the development of scientific branches related to photoelectrochemical cells and photocatalytic processes takes place in parallel. However, the scientific results of each of these fields may be useful in another one. For example, some materials such as metal phosphides were originally used for the electrocatalytic hydrogen evolution. However, these compounds are active co-catalysts for photocatalytic hydrogen production [8]. Titania may be successfully used both as the material for the photoelectrochemical cell and as the photocatalyst [9].

To take into account the achievements in different branches, it is necessary to have a tool that allows comparing some characteristics of the two phenomena. As such a tool, similarity theory can be used, which makes the transition between quantitative characteristics of phenomena of the same nature. The methods of similarity theory are successfully used to describe physical processes in the field of engineering and mechanical engineering. In hydrodynamics, the phenomena of thermal conductivity, diffusion and electrical conductivity in liquids are studied using the similarity theory [10]. The aim of this paper is to determine the possibility of using similarity theory methods to describe the phenomena of photocatalytic hydrogen evolution and photocurrent generation. With the help of the dimension theory, potential similarity criteria were obtained in this work, after which they were used to analyze the literature data.

2. Search of parameters which may be used as similarity criteria

In the study of physical phenomena, a system of concepts and a system of units are introduced. The system of concepts includes the quantities characterizing various aspects of the studied processes, while the system of units determines the numerical values of the introduced characteristics. There are a number of correlations between these characteristics. Any physical relationship between different quantities can be formulated as a relationship between dimensionless quantities. This postulate underlies the theory of dimension [11]. With the help of dimension theory, the parameters that may serve as similarity criteria can be identified. Within the framework of this approach, at the first stage it is necessary to identify the defining system of parameters. At the second stage, linearly independent dimensionless combinations, which are potential similarity criteria, are formed from this system of parameters by analyzing dimensions [11]. At the third stage, the obtained parameters are verified by the experimental data.

Let us apply the theory of dimension to the discussed processes. In the case of photocatalysis, it is necessary to describe quantitatively the reaction system (concentration and nature of reagents, volume of the reaction mixture, concentration of the catalyst or its mass), the light source and the photocatalytic activity of the catalyst. In the case of generating a photocurrent, we will take into account the characteristics of the light source and the photoelectrochemical cell. The irradiation source can be characterized by a set of independent quantities that determine the number of incident light quanta and their energy: the irradiation power and wavelength, the number of incident photons and the wavelength of radiation, the number of incident photons and the energy of one photon, etc. The parameters describing the target properties of the photocatalyst and the photoelectrochemical cell are of the greatest interest.

2.1. Parameters characterizing the photocatalytic activity

The photocatalytic activity describes to what extent the studied system is a photocatalyst. In the literature several parameters describing the catalyst productivity are mentioned, including the catalytic activity [12–21], the turnover number [20–22], the quantum yield [12, 19–21], the quantum efficiency [12, 19–21], the STH (solar-to-hydrogen) [14, 22]. The ways of their calculation were summarized in Table 1.

The catalytic activity, just as in the traditional catalysis, is defined as the rate of the photocatalytic process (W) divided by the catalyst mass (m) [20, 23]. The catalytic activity is often measured in $\mu mol \cdot h^{-1} \cdot g^{-1}$. The catalytic properties of the samples can be characterized by the turnover number (TON).

Table 1 Quantities characterizing the photocatalytic activity of samples.

Quantity	Symbol	Formula	
Catalytic activity	CA	$CA = W/m$	(1)
Turnover number	TON	$TON = \frac{W}{N_{active\ sites}}$ or $TON = \frac{W}{S_{catalyst\ surface}}$	(2)
Quantum yield	ϕ, Φ	$\Phi = \frac{N_{disappearing\ molecules}}{N_{absorbed\ photons}} \cdot 100\%$	(3)
Quantum efficiency	AQE, QE, PE	$AQE = \frac{N_{disappearing\ molecules} \cdot 100\%}{N_{incident\ photons}} = \frac{W \cdot h \cdot c \cdot N_A \cdot 100\%}{P_{irradiation} \cdot S_{irradiation} \cdot \lambda}$	(4)
Solar-to-hydrogen	STH	$STH = \frac{\Delta G^\circ \cdot W \cdot 100\%}{P_{irradiation} \cdot S_{irradiation}} = \frac{AQE \cdot \lambda \cdot \Delta G^\circ}{h \cdot c \cdot N_A}$	(5)

 DOI: 10.15826/chimtech.2023.10.2.03

The TON is the ratio of the number of photoinduced transformations for a given period of time to the number of active sites ($N_{\text{active sites}}$) [21]. However, in heterogeneous catalysis it is difficult to determine the number of active sites; it is often unknown. Therefore, for certainty, when calculating TON, normalization is carried out on the surface area of the catalyst ($S_{\text{catalyst surface}}$).

Since the photocatalytic activity of the samples is directly related to the lighting conditions (type and power of illumination, wavelength), the quantum yield is used to evaluate the photocatalyst productivity and their comparison with each other [12, 19–21]. The quantum yield is a number of defined events, occurring per photon absorbed by the system at a specified wavelength [20, 21]. In heterogeneous photocatalysis, determining the number of absorbed photons is quite difficult: photocatalyst particles reflect and scatter light, and the contribution of this effect is difficult to measure. In practice, apparent quantum efficiency is commonly used; it is normalized per photon incident in the system instead of a photon absorbed by the system. Table 1 shows the formulas for the quantum yield and quantum efficiency calculation when monochromatic light is used.

The photocatalytic reaction is often considered as transformation of the energy of the incident light to the energy of the chemical bonds. From this point of view, the photocatalyst producibility may be estimated using solar-to-hydrogen (STH). During the reaction, $\Delta G^\circ \cdot W$ J transforms to the chemical energy per unit of time, while $P_{\text{irradiation}} \cdot S_{\text{irradiation}}$ J enters the system per unit of time [24]. In general, the ratio between these values is the efficiency of energy conversion during the photocatalytic reaction.

Note that the quantities characterizing the photocatalytic activity can be expressed in terms of a basic set of the certain parameters. This basis includes the photocatalytic reaction rate, the Gibbs energy, the mass and surface area of the catalyst, the irradiation power, and the area of the irradiation surface. Table 1 shows the relationship between these basic parameters and the parameters characterizing the photocatalytic activity. For a complete description of the reacting system, it is necessary to add to these parameters the concentration and nature of the reagents, the volume of the reaction mixture, and the geometric characteristics of the reactor. The example of a basic set of parameters is given in Table 2. This list may be completed as mentioned in the paper [25]; however, this basic set is sufficient for the tasks in the present work.

Special attention should be paid to the values of quantum efficiency and solar-to-hydrogen. They are dimensionless; therefore, they can act as similarity criteria if the conditions of geometric and physical similarity of two reaction systems are fulfilled, for example, for the photocatalytic hydrogen production in reactors of different volumes but the same geometry.

Table 2 Parameters describing the photocatalytic hydrogen production.

Part of the reaction system	Characterizing parameters
The basic set of parameters	
Reagents	Reagent concentration, volume of the reaction mixture
Light source	Irradiation power, surface of irradiation, wavelength
Working photocatalyst	Mass, catalyst surface, reaction rate
Chemical reaction	Gibbs energy
Chemical reactor	Geometric parameters
Similarity criteria	
Reaction system	Quantum efficiency, STH

2.2. Parameters characterizing the efficiency of the photoelectrochemical cell

To describe the efficiency of the photoelectrochemical cells, researchers often use short-circuit current density (J_{sc}) [26–36], open-circuit potential (V_{oc}) [26, 27, 30, 31, 33, 35–37], fill factor (FF) [30, 33, 35, 36, 38], power conversion efficiency (PCE, η) [26–31, 33, 35, 37, 38], incident photon-to-current efficiency (IPCE, external quantum efficiency, EQE) [32, 37–39], solar-to-hydrogen (STH) [26, 28, 31, 39]. Let us consider each of the values in more details.

The short-circuit current density, open-circuit voltage, fill factor, and power conversion efficiency are calculated from the voltammograms (see Figure 1) [40]. The short-circuit current density is known to be the current normalized to the area of illumination that occurs in the cell without any potential [41, 42]. The physical meaning of this value is the highest current density which may be obtained in the photoelectrochemical cell. The short-circuit current density is dependent on the rate of electron-hole pair formation, their diffusion into the semiconductor and in the external circuit [41, 42]. One can say that the J_{sc} indirectly depends on the nature of the semiconductor and electrolyte and the characteristics of the irradiation source.

The open-circuit voltage is the voltage occurring in the cell without any current [40–42]. For the discussed cell whose voltammogram is given in Figure 1 the open-circuit voltage equals ~0.6 V. The open-circuit voltage shows the highest potential which may be obtained in the cell.

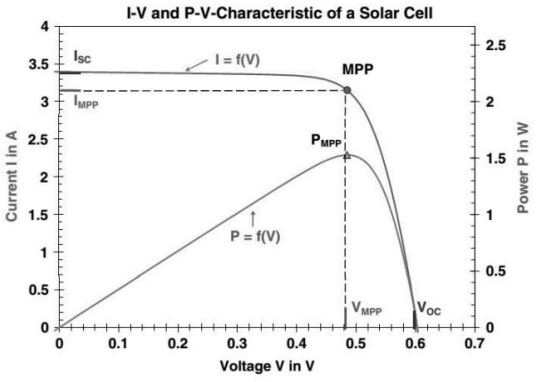

Figure 1 Example of calculation of several characteristics describing the effectivity of the photoelectrochemical cell according to [40].

 DOI: 10.15826/chimtech.2023.10.2.03

The physical meaning of the open-circuit voltage is the efficiency of light energy transformation in one act of photoelectrochemical reaction. This parameter is largely determined by the nature of the chemical processes occurring in the electrolyte solution and at the interface of the electrode/electrolyte [42].

The fill factor is the value reflecting the impact of the resistance of the photoelectrochemical cell and showing the degree of deviation of the produced cell power from the possible one without any resistance. The fill factor is calculated as the ratio of maximum power to the product of the short-circuit current density and the open-circuit voltage:

$$\mathrm{FF} = \frac{J_{\mathrm{MPP}} \cdot V_{\mathrm{MPP}}}{J_{\mathrm{SC}} \cdot V_{\mathrm{OC}}} \cdot 100\%, \quad (6)$$

where FF is the fill factor, J_{MPP} is the current density in which the highest power is generated, V_{MPP} is the potential in which the highest power is generated, J_{sc} is the short-circuit current density, and V_{OC} is the open-circuit potential. As shown in Figure 1, the plot of the produced power from potential was constructed, after which the maximum point (MPP) was found. The higher the fill factor, the closer the shape of the current-voltage curve to a rectangular one. The deviation from this shape is caused by resistance in the photoelectrochemical system, recombination of electron-hole pairs [42], and changing resistance at the interface electrode/electrolyte [41]. Because the fill factor is a dimensionless quantity, it can be used as the similarity criterion for the photoelectrochemical systems, for example, in case of scaling the photoelectrochemical cells.

The power conversion efficiency of the photoelectrochemicall cell shows the ratio of the electrical energy produced in the cell to the energy of the incident light [43]:

$$\eta = \frac{J_{MPP} \cdot V_{MPP}}{P_{irradiation}} \cdot 100\% = \frac{J_{SC} \cdot V_{OC} \cdot FF}{P_{irradiation}} \cdot 100\%, \quad (7)$$

where η is the power conversion efficiency, J_{MPP} is the current density in which the highest power is generated, V_{MPP} is the potential in which the highest power is generated, $P_{\mathrm{irradiation}}$ is the power of the irradiation which incidents on the photoelectrochemical cell, J_{sc} is the short-circuit current density, V_{OC} is the open-circuit potential, and FF is the fill factor. The power conversion efficiency shows the efficiency of the energy transformation. PCE is a dimensionless quantity and can act as the similarity criterion for the photoelectrochemical systems.

The incident photon-to-current efficiency is defined as the number of produced electrons divided by the number of photons incident in the system [43]. By simple transformations, one can obtain Equation (8), relating the short-circuit current density and irradiation power. Of practical value is the dependence of IPCE on the wavelength, which makes it possible to optimize the irradiation conditions of the photoelectrochemical cell.

$$IPCE = \frac{N_{\mathrm{electrons}}}{N_{\mathrm{photons}}} \cdot 100\% = \frac{J_{\mathrm{SC}} \cdot h \cdot c}{P_{\mathrm{irradiation}} \cdot e \cdot \lambda} \cdot 100\%, \quad (8)$$

where IPCE is the incident photon-to-current efficiency, $N_{\mathrm{electrons}}$ is the number of electrons generated in the cell, N_{photons} is the number of photons incident in the system, J_{sc} is the short-circuit current density, $P_{\mathrm{irradiation}}$ is the power of irradiation incident on the photoelectrochemical cell, h is Planck's constant, c is the speed of light, e is the electron charge, and λ is the wavelength of the incident irradiation.

If additional water decomposition and hydrogen evolution occur in the photoelectrochemical cell, the efficiency of this process can be estimated using solar to hydrogen (STH), which may be calculated according to the following equation:

$$\mathrm{STH} = \frac{J_{\mathrm{SC}} \cdot 1.23 \cdot \eta_{\mathrm{F}}}{P_{\mathrm{irradiation}}} \cdot 100\%, \quad (9)$$

where J_{sc} is short-circuit current density, η_{F} is the Faraday efficiency factor for hydrogen evolution, and $P_{\mathrm{irradiation}}$ is the power of irradiation incident on the photoelectrochemical cell. It should be noted that the STH parameter can also characterize the photocatalytic hydrogen production (see 2.1 and Equation 5). In this case, STH shows the relationship between the energy of hydrogen production over the photocatalyst and the energy of incident light. In the case of the photoelectrochemical cell, STH reveals the share of the light energy which was used for the water decomposition and contained the product of the rate of electrochemical hydrogen production ($J_{SC} \cdot \eta_F$) and the Gibbs energy of this reaction (1.23 V for water decomposition), as shown in the Equation 9. So, these values have the same physical meaning for both different processes.

As in the case of the photocatalytic hydrogen evolution, the quantities characterizing the efficiency of the photoelectrochemical cell can be expressed in terms of the basic set of several parameters. The short-circuit current density, the open-circuit potential, the current density at which the cell generates maximum power (in this case, V_{MPP} is determined from the experimental data, the maximum cell power can act as the similarity criterion), the irradiation power, the area of the illuminated part of the photoelectrochemical cell, the irradiation wavelength (for simplicity, we restrict our consideration to monochromatic radiation). To fully characterize the reacting system, it is necessary to add to these parameters the concentration and nature of the electrolyte, the nature of the electrodes, and the geometric design of the cell.

Among the quantities used by researchers to describe the efficiency of the photoelectrochemical cell, several dimensionless parameters can be selected: the fill factor, the power conversion efficiency, the incident photon-to-current efficiency, and the solar-to-hydrogen. These parameters can act as the similarity criteria provided that the conditions of geometric and physical similarity of two photoelectrochemical cells are met.

 DOI: 10.15826/chimtech.2023.10.2.03

2.3. Derivation of the similarity criteria that may be used for the description of relation between the efficiencies of the photocatalytic hydrogen production and the photoelectrochemical cell

The analysis of the nature of the photocatalytic hydrogen production and the photocurrent generation shows that these phenomena are analogous to each other [7]. Therefore, their quantitative description uses analogous values whose combination may be serve as the similarity criteria making the transition between the descriptions of both phenomena.

Let us consider the list of the analogous quantities (see Table 3) in detail. The quantities used for the description of the photocatalytic hydrogen evolution and the photoelectrochemical cell allow defining the change in the number of molecules or the number of the electric charges per unit of time. In both cases, these changes are caused by the change in the number of electrons taking part in the target processes. Based on the dimensions, the changing electron amount during the photocatalytic hydrogen production per unit of time per unit of irradiation surface may be calculated as $2 \cdot W \cdot N_A \cdot S_{irradiation}^{-1}$, while the changing electron amount during the photocurrent generation per unit of time per the surface of the photoelectrochemical cell may be defined as J_{SC}/e. The ratio of these quantities will be dimensionless and may act as the similarity criterion. The validity of this statement will be verified below by analyzing the literature data. It should be noted that voltammograms are often not presented in the literature, while most articles are accompanied by the data on the change in current density over time generated at the constant potential. This quantity, e.g., at the first cycle, may be used instead of the short-circuit current density, because it was measured at the constant potential and has the same dimension. In this case, the similarity criterion was labeled as Q_1'.

The photocatalytic hydrogen production and the photocurrent generation are considered as the conversion of light energy into chemical bond or electrical energy. Therefore, these phenomena may be characterized by the energy converted per unit of time. As in the previous case, for the photocatalytic reaction, it is necessary to normalize by the area of the illuminated part of the reactor, since such accounting occurs when the efficiency parameters of the photoelectrochemical cell are measured. Based on dimensions, we obtain formulas for estimating the amount of energy converted per unit of time per unit of area of the illuminated systems. They will be $\frac{\Delta G^\circ \cdot W}{S_{\text{irradiation}}}$ and $J_{SC} \cdot V_{OC}$ for the photocatalytic hydrogen production and the photoelectrochemical cell, respectively. The ratio of these quantities will be dimensionless and may serve as the similarity criterion Q_2.

The studied phenomena occur in the light. From this point of view, the photocatalytic hydrogen evolution may be characterized by the quantum efficiency, while the photocurrent generation is described by ICPE. Both values are dimensionless, and their ratio is dimensionless too and may serve as a similarity criterion:

$$Q_3 = \frac{AQE}{IPCE} = \frac{W \cdot N_A \cdot e}{J_{SC} \cdot S_{\text{irradiation}}} = \frac{Q_1}{2}, \quad (10)$$

$$Q_3' = \frac{AQE}{IPCE} = \frac{W \cdot N_A \cdot e}{J \cdot S_{\text{irradiation}}} = \frac{Q_1'}{2}. \quad (11)$$

Note that the criteria Q_1 and Q_3 differ a constant multiplier. It is known that multiplying the similarity criterion by a number allows getting another similarity criterion [11].

The efficiencies of the photocatalytic hydrogen production and the photocurrent generation are characterized by the solar-to-hydrogen and the power conversion efficiency, respectively.

Table 3 Quantities describing the similar aspects of the photocatalytic hydrogen production and the photocurrent generation in the photoelectrochemical cell.

Quantity	Hydrogen production	Photocurrent generation in the cell	Possible similarity criterion
Change in electron amount per unit of time per irradiation surface	$\frac{2 \cdot W \cdot N_A}{S_{irradiation}}$	$\frac{J_{SC}}{e}$	$Q_1 = \frac{2 \cdot W \cdot N_A \cdot e}{J_{SC} \cdot S_{irradiation}}$
		$\frac{J}{e}$	$Q_1' = \frac{2 \cdot W \cdot N_A \cdot e}{J \cdot S_{\text{irradiation}}}$
Energy converted per unit of time per unit of irradiation surface	$\frac{\Delta G^\circ \cdot W}{S_{irradiation}}$	$J_{SC} \cdot V_{OC}$	$Q_2 = \frac{\Delta G^\circ \cdot W}{S_{\text{irradiation}} \cdot J_{SC} \cdot V_{OC}}$
Efficiency of using light	Quantum efficiency	IPCE	$Q_3 = \frac{AQE}{IPCE} = \frac{W \cdot N_A \cdot e}{J_{SC} \cdot S_{\text{irradiation}}} = \frac{Q_1}{2}$ $Q_3' = \frac{AQE}{IPCE} = \frac{W \cdot N_A \cdot e}{J \cdot S_{\text{irradiation}}} = \frac{Q_1'}{2}$
Efficiency of energy conversion	STH	η	$Q_4 = \frac{STH}{\eta}$

 DOI: 10.15826/chimtech.2023.10.2.03

Dividing these two parameters by each other yields the similarity criterion Q_4:

$$Q_4 = \frac{STH}{\eta} = \frac{\Delta G^\circ \cdot W}{S_{\text{irradiation}} \cdot J_{SC} \cdot V_{OC} \cdot FF}. \quad (12)$$

Thus, four potential similarity criteria were obtained. Since the first and the third, the second and the fourth criteria differ by a constant multiplier, in order to find out whether the proposed values are the similarity criteria, it is enough to verify only the parameters Q_1 and Q_2.

3. Checking the possibility of applying the criterion Q_1' as the similarity criterion

To check whether the proposed values are similarity criteria, some literature data was analyzed [45–81]. It should be noted that the data of linear voltammetry either were not given by the authors or differ from the form shown in Figure 1. So, the current density in the cell at the constant potential value, measured by chronoamperometry, will be used for comparison instead of the short-circuit current density. From the point of view of dimension theory, such substitution is correct due to the same dimensions of both quantities (mA/cm²). Thus, in most of the reviewed data, the possibility of using the parameter Q_1' as the similarity criterion was verified.

In the theory of similarity, a geometric level of similarity and a physical one are often distinguished [44]. The geometric level implies an identical shape of particles and/or elements of the reaction set-up, its characteristic sizes [44]. When moving from the study of photocatalytic hydrogen evolution to measuring photocurrents for two different samples, the similarity at the geometrical level is often preserved. It is due to the comparable particle sizes of the tested samples, the experimental set-ups for studying the photocatalytic hydrogen evolution and the photoelectrochemical properties are the same. Special attention should be paid to the morphology of the samples: in case of its change, the conditions of the geometric similarity are violated. If the geometric similarity is observed for the studied systems, then the similarity of phenomena can also be taken place at the physical level. Two phenomena are similar if all parameters characterizing them are similar [44]. It means that the samples should be tested under the same conditions, such as power irradiation, its wavelength, the composition of electrochemical cells and electrolyte, the composition of catalysts, etc. If these conditions are fulfilled, the question of similarity of the photocatalytic hydrogen production and the photocurrent generation for the studied samples can be considered.

Below there are data on catalysts of various chemical nature, solid solutions of different compounds, the series of samples in which the mass ratio of the components is changed; the photocatalytic and photovoltaic characteristics were studied in solutions of different electrolytes. All discussed data are given in Tables 4–7. Each table contains the experimental conditions; the criterion Q_1' was calculated. The error in calculating the parameter was determined taking into account the instrumental errors of the methods. They were either for 10% (if quantitative data were taken from tables or from the text), or for 15% in the case of getting data from the figures.

3.1. Solid solutions of different compounds

The data on the photocatalytic hydrogen production and photocurrent generation over some solid solutions are given in Table 4 [45–52]. The solid solutions of cadmium sulfide and zinc sulfide were described in a number of works. The short-circuit current densities were measured in [45] and [46], and the similarity criterion Q_1 was calculated from obtained data. The ratio of the number of electrons used for the photocatalytic hydrogen evolution and those to the number of electrons taking part in the photocurrent generation remained constant within experimental errors for all samples, except for zinc sulfide in [45]. Probably, zinc sulfide should be considered separately due to low absorbance of visible light and different chemical nature (see Section 3.2). The authors of [46] studied a wider range of the solid solution composition; however, in this case, no indication of change in the parameter Q_1 could be identified. Perhaps, it was caused by different composition of the electrolytes used in the experiments. The mixture of Na_2S and Na_2SO_3 was used for the photocatalytic hydrogen production while sodium polysulfide was chosen for the photoelectrochemical experiments. In both cases, chemical transformations occurred between charge carriers and electrolytes. However, various chemical processes were realized, so the changes in the target parameters vs. the photocatalyst composition were different. In this case, it was impossible to apply the similarity theory due to the violation of the condition of physical similarity. S. Du et al. studied the solid solutions of cadmium sulfide and cadmium selenides with low Se content [47]. The dependences of the photocatalytic hydrogen production rate and the current density on selenium concentration have a bell-shaped form, while the electron ratios expressed by the criterion Q_1' stayed the same and were 300–400 within the experimental errors.

The solid solutions of CdS and MnS were described in [48]. The dependences of both target characteristics on the solid solution composition went through a maximum. The Q_1' criteria were calculated for the tested samples and given in Table 4. One can see that Q_1' doubles when cadmium sulfide forms solid solutions with manganese sulfide. It may be associated with the changes in the rate constants of photochemical processes and charge recombination depending on the chemical nature of semiconductor. The ratio between the numbers of electrons used for the photocatalytic hydrogen evolution and those taking part in the photocurrent generation remained constant for all samples, excluding the photocatalyst with x = 0.9. For the mentioned sample, the deviation was due to its chemical nature. This photocatalyst

 DOI: 10.15826/chimtech.2023.10.2.03

was a composite consisting of MnS and the solid solution of cadmium sulfide and manganese sulfide [48]. So, in this case, we deal with the non-compliance with the conditions of the physical similarity of the systems discussed. The same behavior was found for $Mn_xCd_{1-x}S$ [49]. For the solid solutions with different ratios of manganese to cadmium, the Q_1' criterion remained a constant within the experimental error, while it increased by almost two times in the transition from CdS to the solid solution of cadmium and manganese sulfides.

The solid solutions of more complex composition such as $Cd_{1-x}Zn_xS$ and $Cd_{1-x}Zn_xMo_yS_{1+2y}$ were mentioned in [50]. The introduction of the solid solution in the structure changed its chemical composition, affecting both the change in the target characteristics and their ratios. In this case, the condition of the physical similarity of the samples was violated, and it is incorrect to talk about the application of similarity theory. The $ZnFe_2O_4$ and $ZnGaO_4$ spinels and their solid solutions were described in [51]. The ratio between the numbers of electrons used for the photocatalytic hydrogen evolution and those taking part in the photocurrent generation varied for these samples due to different chemical nature. For the solid solutions based on $ZnFe_2O_4$ and $ZnGaO_4$, ratios of the number of electrons used for the photocatalytic hydrogen evolution to the number of electrons taking part in the photocurrent generation were less than those for individual compounds. However, their differences between each other were more than 10%, which may be due to the formation of oxygen vacancies for the samples with $x>1$. Therefore, four samples demonstrated different physicochemical properties, and the similarity theory is not applicable to this case. In the work [52], the authors studied the photocatalysts consisting of the solid solutions of zinc sulfide, chromium sulfide, indium sulfide with different Q_1' values.

Note that for the samples with adjacent values of metal content (e.g., Zn:Cr = 85:15 and Zn:Cr = 75:25) the target criteria are the same within the experimental errors. Perhaps, it is connected with a stronger influence on the electronic structure of small changes in the composition of the triple solid solutions, which cause significant changes in the physicochemical properties and do not allow considering the samples similar. In the case of small fluctuations in the chemical composition, we can only talk about partial similarity of the discussed systems.

To sum up, for binary solid solutions, the criterion Q_1' can serve as the similarity criterion in case of compliance with the conditions of physical and geometric similarity. For triple solid solutions, the change in the photocatalyst composition has a stronger effect on its physicochemical properties, as a result of which we can only talk about partial similarity for the samples similar in composition. For transition from individual compounds to their solid solutions, the Q_1' criterion may both retain its value and change. Such cases should be considered individually.

3.2. Samples whose chemical nature were different

The data obtained over the samples whose chemical composition was changed during the preparation were given in Table 5 ([53–74]). For compounds with different chemical nature**,** the transition from the photocatalysts to the photoelectrodes was accompanied by the different ratio of the number of electrons used for photocatalytic hydrogen production to the number of electrons taking part in the photocurrent generation. For instance, in [53] NH_2-UiO-66 and $ZnIn_2S_4$ were studied, and for them the Q_1' criterion differed by 7 times, while for CdS and ZnS – by 5 times [45]. This result was not surprising because the number of electrons was largely determined by the balance between the rate of charge generation, their recombination, and consumption in various processes. For samples with different chemical nature, the rate constants of these stages differed, and the ratios also diverged. In terms of the similarity theory, one can say that in this case the conditions of physical similarity were violated. More interesting were the cases in which the chemical composition of the catalyst was changed by loading additional compounds or doping. Did the Q_1'criterion change in this case?

A special case of modification of the semiconductor was capping some ligands on the photocatalyst surface. In [54] titanium dioxide with capped quantum dots based on cadmium selenide and the solid solution of cadmium sulfide and zinc sulfide using ammonium thiocyanide and mercaptopropionic acid was described. The scheme for the functioning of these photocatalysts was proposed, in which photogenerated holes were transferred from the valence band of quantum dots to the highest occupied molecular orbital of the ligand [54]. As a result, the target characteristics of the photocatalysts prepared with diverse ligands differed. Simultaneously, the Q_1' criteria showing the number of electrons used for the photocatalytic hydrogen evolution divided by the number of electrons taking part in the photocurrent generation differed. Possibly, it may be assisted with strong differences in the transfer constants of the photogenerated holes, which had an indirect effect on the number of electrons in the discussed systems.

The photocatalyst surface was often modified by loading compounds and forming the composite catalysts. The researchers extensively studied the composites with different composition. In [55] cadmium sulfide whose surface was modified with Nb_2CT was studied. This deposition led to the increase in the reaction rate by 1.7 times, while the photocurrent grew by 1.8 times. The ratio of the number of electrons occurring in the photocatalytic hydrogen production to the number of electrons used for the photocurrent generation was the same for these samples. In [56] copper nanoparticles and their role in the photocatalysis after deposition on the surface of bohrium nitride, polyaniline, and the composite photocatalyst consisting of bohrium nitride and polyaniline were discussed. Copper nanoparticles and copper nanoparticles deposited on BN demonstrated the same catalytic activity.

 DOI: 10.15826/chimtech.2023.10.2.03

Table 4 Verifying the possibility of using Q_1' as the similarity criterion for the series of different solid solutions.

No.	Sample	Photocatalyst	Sacrificial agent	*W* (μmol/min)	Counter and reference electrodes	Electrolyte	Current density (mA/cm²)	Light source	Q_1'	Ref
1	CdS	Solid solutions of CdS and ZnS	0.24 M Na_2S, 0.35 M Na_2SO_3	0.08	Pt/C	10 vol.% ethanol, 0.5 M NaOH	0.150	Xe lamp	0.14±0.02	[45][a]
	$Cd_{0.25}Zn_{0.75}S$			0.62			0.767		0.22±0.03	
	$Cd_{0.35}Zn_{0.65}S$			0.48			0.992		0.13±0.02	
	$Cd_{0.65}Zn_{0.35}S$			0.57			0.958		0.16±0.02	
	ZnS			0.10			0.975		0.027±0.004	
2	CdS	Solid solutions of CdS and ZnS	0.1 M Na_2S, 0.1 M Na_2SO_3	0.12	Cu_2S/brass	1 M Na_2S_n, 0.1 M NaCl	0.881	450-LED	0.44±0.06	[46]
	$Cd_{0.9}Zn_{0.1}S$			0.29			0.901		1.0±0.1	
	$Cd_{0.8}Zn_{0.2}S$			0.37			2.21		0.54±0.08	
	$Cd_{0.7}Zn_{0.3}S$			0.47			1.37		1.1±0.2	
	$Cd_{0.6}Zn_{0.4}S$			0.39			0.33		3.8±0.5	
	$Cd_{0.5}Zn_{0.5}S$			0.55			0.067		26±4	
	$Cd_{0.4}Zn_{0.6}S$			0.96			0.139		22±3	
	$Cd_{0.3}Zn_{0.7}S$			2.25			0.984		7±1	
	$Cd_{0.2}Zn_{0.8}S$			0.96			0.259		12±2	
	$Cd_{0.1}Zn_{0.9}S$			0.56			0.128		14±2	
	ZnS			0.025			0.024		3.3±0.5	
3	CdS	Solid solutions of cadmium sulfide and cadmium selenide	5 vol.% lactic acid	0.35	Pt, $Hg\|Hg_2Cl_2\|Cl^-$	0.5 M Na_2SO_4	0.0036	Xe lamp	308±43	[47][a]
	$CdS_{0.99}Se_{0.01}$			0.55			0.0038		466±66	
	$CdS_{0.975}Se_{0.025}$			0.61			0.0058		335±47	
	$CdS_{0.95}Se_{0.05}$			1.22			0.0100		391±55	
	$CdS_{0.925}Se_{0.075}$			0.61			0.0064		306±43	
	$CdS_{0.9}Se_{0.1}$			0.36			0.0027		425±60	
4	x = 0	$Mn_xCd_{1-x}S$	10 vol.% lactic acid	0.35	Pt, $AgCl\|Ag\|Cl^-$	0.2 M Na_2SO_4	0.015	Xe lamp	74±10	[48]
	x = 0.3			1.02			0.021		155±22	
	x = 0.5			1.50			0.024		199±28	
	x = 0.6			1.88			0.032		188±26	
	x = 0.9			0.59			0.002		939±132	
5	CdS	Solid solutions of cadmium sulfide and manganese sulfide	20 vol.% lactic acid	0.055	Pt, $AgCl\|Ag\|Cl^-$	0.1 M Na_2SO_4	0.03	Xe lamp	5.9±0.8	[49]
	MCS-1			0.152			0.043		11±2	
	MCS-2			0.178			0.065		9±1	
	MCS-3			0.127			0.04		10±1	
	MCS-4			0.117			0.035		10±2	
6	ZCS	Solid solutions of ZnS, CdS, MoS_2	0.35 M Na_2S, 0.35 M Na_2SO_3	0.0003	Pt, $AgCl\|Ag\|Cl^-$	0.5 M Na_2SO_4	0.00014	Xe lamp	8±1	[50]
	ZCM_5S			0.0038			0.00021		58±8	

DOI: 10.15826/chimtech.2023.10.2.03

Table 4 Verifying the possibility of using Q_1' as the similarity criterion for the series of different solid solutions (continued).

No.	Sample	Photocatalyst	Sacrificial agent	*W* (μmol/min)	Counter and reference electrodes	Electrolyte	Current density (mA/cm²)	Light source	Q_1'	Ref
7	x = 0	$ZnFe_{2-x}Ga_xO_4$	10 vol.% triethanolamine	4.63	Pt, AgCl|Ag|Cl⁻	0.5 M Na_2SO_4	0.0002	Xe lamp	$(7\pm1)\cdot10^4$	[51]
	x = 0.5			5.40			0.00075		$(2.3\pm0.3)\cdot10^4$	
	x = 1.5			5.85			0.00050		$(3.7\pm0.5)\cdot10^4$	
	x = 2.0			5.98			0.0017		$(11\pm2)\cdot10^4$	
8	ZIS	Solid solutions of zinc sulfides, chromium sulfide, indium sulfide	0.25 M Na_2S, 0.35 M Na_2SO_3	0.74	C, Hg|Hg_2Cl_2|Cl^-	0.5 M Na_2SO_4	0.00007	Xe lamp	$(3.4\pm0.5)\cdot10^4$	[52]
	$Z_{0.85}C_{0.15}IS$			1.35			0.00015		$(2.9\pm0.4)\cdot10^4$	
	$Z_{0.75}C_{0.25}IS$			1.71			0.00022		$(2.5\pm0.4)\cdot10^4$	
	$Z_{0.55}C_{0.45}IS$			1.09			0.00008		$(4.4\pm0.6)\cdot10^4$	

[a] In this work the short-circuit current densities were presented, Q_1 was calculated.

Table 5 Verifying the possibility of using Q_1' as the similarity criterion for the series of samples with different chemical nature.

No.	Sample	Photocatalyst	Sacrificial agent	W (μmol/min)	Counter and reference electrodes	Electrolyte	Current density (mA/cm²)	Light source	Q_1'	Ref
Different chemical compounds										
1	NU66d	NH_2-UiO-66 decarboxylated	0.25 M Na_2S/0.35 M Na_2SO_3	0.050	Pt, AgCl|Ag|Cl^-	0.1 M Na_2SO_4	0.0028	Xe lamp, λ ≥ 420 nm	57±8	[53]
	ZIS	$ZnIn_2S_4$		0.072			0.0058		395±56	
	NU66/ZIS-30	$ZnIn_2S_4$ deposited on NH_2-UiO-66		0.85			0.0078		349±49	
	NU66-d/ZIS-30	$ZnIn_2S_4$ deposited on decarboxylated NH_2-UiO-66		1.22			0.0091		428±60	
2	CdS	CdS	0.24 M Na_2S, 0.35 M Na_2SO_3	0.08	Pt/C	10 vol.% ethanol, 0.5 M NaOH	0.150	Xe lamp	0.14±0.02	[45]
	ZnS	ZnS		0.10			0.975		0.027±0.004	
Capping ligands on the photocatalyst surface										
3	SCN	TiO_2 with capping quantum dots using NH_4SCN	0.1 M ascorbic acid	4755	Pt, AgCl|Ag|Cl^-	0.1 M ascorbic acid	0.053	AM-1.5G	$(2.9\pm0.4)\cdot10^5$	[54]
	MPA	TiO_2 with capping quantum dots using mercaptopropionic acid		470			0.028		$(53.7\pm0.8)\cdot10^3$	
Deposition of different compounds										
4	CdS	CdS	10 vol.% lactic acid	0.52	Pt, AgCl|Ag|Cl^-	1 M Na_2SO_4	0.033	Xe lamp, λ ≥ 420 nm	501±71	[55]
	CdS/Nb_2CT-60	CdS with deposited Nb_2CT (60 mg)		0.90			0.062		465±65	
5	Cu/BN@PANI-2.5 wt.%	2.5% Cu deposited on BN and polyaniline	14 vol.% lactic acid	0.52	Pt	0.1 M KOH	49	Xe lamp, λ ≥ 420 nm	0.034±0.005	[56]
	Cu-PANI/2.5%	2.5% Cu deposited on polyaniline		0.25			30		0.027±0.004	
	Cu/BN-2.5%	2.5% Cu deposited on BN		0.19			19		0.032±0.005	
	Cu NPs	Cu		0.165			15		0.035±0.005	

DOI: 10.15826/chimtech.2023.10.2.03

Table 5 Verifying the possibility of using Q_i' as the similarity criterion for the series of samples with different chemical nature (continued).

No.	Sample	Photocatalyst	Sacrificial agent	W (μmol/min)	Counter and reference electrodes	Electrolyte	Current density (mA/cm²)	Light source	Q_i'	Ref
6	NiCo-LDH	Nickel-cobalt double layered hydroxides	0.2 M Na_2S, 0.2 M Na_2SO_3	0.13	Pt, AgCl|Ag|Cl^-	0.5 M Na_2SO_4	0.48	AM-1.5G	0.9±0.1	[57]
	CoO	CoO		0.20			0.88		0.7±0.1	
	CoO/NiCo-LDH	CoO deposited on nickel-cobalt double layered hydroxides		1.00			3.15		1.0±0.1	
7	ZnS/PDA1	Polydopamine deposited on ZnS	0.35 M Na_2S, 0.25 M Na_2SO_3	0.36	Pt, AgCl|Ag|Cl^-	0.5 M Na_2SO_4	0.002	Xe lamp	577±81	[58]
	ZnS	ZnS		0.16			0.001		526±74	
8	UiO-66	UiO-66	10 vol.% triethanolamine	0.067	Pt, AgCl|Ag|Cl^-	0.5 M Na_2SO_4	0.02	Xe lamp, λ ≥ 420 nm	11±2	[59]
	UiO-66/NiS_2-5	UiO-66 with deposited 5 wt.% NiS_2		0.30			0.07		14±2	
9	CPt-14	Pt/g-C_3N_4	10 vol.% triethanolamine	3.38	Pt, AgCl|Ag|Cl^-	0.5 M Na_2SO_4	0.00014	Xe lamp, λ ≥ 400 nm	$(8±1)·10^4$	[60]
	CPtO-6	PtO/g-C_3N_4		4.46			0.00020		$(7±1)·10^4$	
10	CdS	CdS	0.35 M Na_2S/0.25 M Na_2SO_3	198	Pt, AgCl|Ag|Cl^-	0.5 M Na_2SO_4	0.0024	Xe lamp, λ ≥ 420 nm	$(2.6±0.4)·10^5$	[61]
	0.4QD/CdS	0.4 wt.% C (quantum dots) deposited on CdS		309			0.0048		$(2.1±0.3)·10^5$	
11	Pt/SiO_2	RP/Pt/SiO_2	–	200.4	Pt, AgCl|Ag|Cl^-	0.5 M Na_2SO_4	0.0030	Xe lamp, λ ≥ 420 nm	21±3	[62]
	CoP2-6	RP/CoP2(6)/SiO_2		401.4			0.0032		40±6	
12	20 WN/CdS	20 WN/CdS	10 vol.% lactic acid	4.02	Pt, AgCl|Ag|Cl^-	0.5 M Na_2SO_4	0.0021	Xe lamp, λ ≥ 420 nm	6218±877	[63]
	CdS	CdS		0.43			0.0005		2771±391	
13	3DOMM-TiO_2	TiO_2 prepared by the template method	10 vol.% methanol	0.136	Pt, AgCl|Ag|Cl^-	0.5 M Na_2SO_4	0.20	Xe lamp, λ ≥ 420 nm	2.2±0.3	[64]
	3DOMM-TiO_{2-x}	TiO_2 prepared by the template method and reduced by $NaBH_4$		0.173			0.31		1.8±0.3	
	3DOMM-TiO_2–*x*@PANI	TiO_2 prepared by the template method with deposited polyaniline		0.264			0.80		1.1±0.1	
	Ag@3DOMM-TiO_{2-x}@PANI	TiO_2 prepared by the template method with deposited polyaniline and Ag		0.281			1.12		0.8±0.1	
14	BCN	C_3N_4 prepared by the thermal polymerization	20 vol.% triethanolamine	0.01	Pt, AgCl|Ag|Cl^-	0.5 M Na_2SO_4	0.0002	Xe lamp	160±23	[65]
	CAN	C_3N_4 prepared by the template method		0.02			0.0004		173±24	
	10% Co/CAN	10% Co_3O_4 deposited on C_3N_4 prepared by the template method		0.04			0.0013		97±13	
15	In_2S_3	In_2S_3	10 vol.% lactic acid	0.0015	Pt, Hg|Hg_2Cl_2|Cl^-	0.5 M Na_2SO_4	0.00055	Xe lamp	9±1	[66]
	25MPIS	25% MoP/In_2S_3		0.24			0.0016		481±68	
16	CdS	CdS	20 vol.% lactic acid	0.44	Pt, AgCl|Ag|Cl^-	0.1 M Na_2SO_4	0.005	Xe lamp, λ ≥ 420 nm	$(2.8±0.4)·10^2$	[67]
	11% Fe_2P/CdS	11% Fe_2P/CdS		34.6			0.070		$(1.6±0.2)·10^3$	

DOI: 10.15826/chimtech.2023.10.2.03

Table 5 Verifying the possibility of using Q_1' as the similarity criterion for the series of samples with different chemical nature (continued).

No.	Sample	Photocatalyst	Sacrificial agent	W (μmol/min)	Counter and reference electrodes	Electrolyte	Current density (mA/cm²)	Light source	Q_1'	Ref
17	TiO_2	TiO_2	0.5 M Na_2S/Na_2SO_3	0.009	Pt, AgCl|Ag|Cl^-	0.5 M Na_2S/Na_2SO_3	0.10	Xe lamp	0.29±0.04	[68]
	CBT-0	CdS/TiO_2		0.489			0.52		3.0±0.4	
18	LTO	$La_2Ti_2O_7$	10 vol.% triethanolamine	0.06	Pt, AgCl|Ag|Cl^-	1 M NaOH	0.012	AM-1.5G	15±2	[69]
	rGO/LTO	71 wt.% reduced graphene oxide deposited on $La_2Ti_2O_7$		0.29			0.026		36±5	
	LTO/Ni-Fe	$La_2Ti_2O_7$ deposited on nickel-iron-double layered hydroxides		0.36			0.034		33±5	
	rGO/LTO/NiFe	Graphene oxide deposited on $La_2Ti_2O_7$ deposited on nickel-iron-double layered hydroxides		0.53			0.068		25±4	
Doping										
19	CdS	CdS	20 vol.% $C_3H_6O_3$	0.84	Pt, Hg|Hg_2Cl_2|Cl^-	0.5 M Na_2SO_4	0.027	Xe lamp, λ ≥ 420 nm	100±14	[70]
	Mo-CdS	CdS:Mo (25 mol.%)		4.87			0.116		134±19	
20	ZnO	ZnO doped with Al	–	0.034	Pt, AgCl|Ag|Cl^-	0.1 M NaOH	0.06	Light source simulating solar light / sunlight	1.8±0.3	[71]
	ZnO/Al/0.5			0.056			0.11		1.6±0.2	
	ZnO/Al/1			0.122			0.24		1.6±0.2	
	ZnO/Al/5			0.183			0.38		1.5±0.2	
21	BCN	Carbon nitride	20 vol.% methanol	0.054	Pt, AgCl|Ag|Cl^-	0.1 M Na_2SO_4	0.00036	Xe lamp, λ ≥ 420 nm	476±67	[72]
	PTCN	Carbon nitride doped by phosphorous		0.092			0.00043		685±97	
22	GCN-B	Carbon nitride	20 vol.% triethanolamine	0.0024	Pt, AgCl|Ag|Cl^-	0.1 M Na_2SO_4	0.18	Xe lamp, λ ≥ 420 nm	$(4.3±0.6)·10^{-2}$	[73]
	GCN-NS	Carbone nitride, nanosheets		0.0083			0.43		$(6±1)·10^{-2}$	
	B,Cs CN-B	Carbon nitride doped with B and Cs		0.0027			0.175		$(5.0±0.7)·10^{-2}$	
	B,Cs CN-NS	Carbon nitride doped with B and Cs, nanosheets		0.0189			0.63		$(10±1)·10^{-2}$	
23	CN	Carbon nitride	10 vol.% triethanolamine	0.29	Pt, AgCl|Ag|Cl^-	0.2 M Na_2SO_4	0.11	Xe lamp, λ ≥ 420 nm	8±1	[74]
	BQCN	Carbon nitride with benzoquinone as linker		0.66			0.25		8±1	

DOI: 10.15826/chimtech.2023.10.2.03

Table 6 Verifying the possibility of using Q1' as the similarity criterion for the series of samples with different weight ratio of the components or preparation time.

No.	Sample	Photocatalyst	Sacrificial agent	W (μmol/min)	Counter and reference electrodes	Electrolyte	Current density (mA/cm²)	Light source	Q_i'	Ref
1	CoP2-4 CoP2-6 CoP2-8	$RP/CoP_2(4)/SiO_2$ $RP/CoP_2(6)/SiO_2$ $RP/CoP_2(8)/SiO_2$	–	401.4 707.4 622.8	Pt, AgCl|Ag|Cl^-	0.5 M Na_2SO_4	0.032 0.052 0.048	Xe lamp, λ ≥ 420 nm	40±6 44±6 42±6	[62]
2	6% MoS_2/CdS 20% MoS_2/CdS	6% MoS_2/CdS 20% MoS_2/CdS	10 vol.% lactic acid	10.62 5.80	Pt, AgCl|Ag|Cl^-	0.5 M Na_2SO_4	0.0036 0.0018	Xe lamp, λ ≥ 420 nm	$(9±1)·10^3$ $(10±2)·10^3$	[75]
3	0% $LaVO_4$ 10% $LaVO_4$ 15% $LaVO_4$ 20% $LaVO_4$ 25% $LaVO_4$	Carbon nitride with different wt. content of deposited $LaVO_4$	10 vol.% triethanolamine	0.027 0.061 0.093 0.041 0.015	Pt, AgCl|Ag|Cl^-	0.1 M Na_2SO_4	0.00045 0.0010 0.0013 0.00075 0.00034	Xe lamp	190±40 196±42 230±49 176±37 144±31	[76]
4	SIS-ZIS-0.1 SIS-ZIS-0.2 SIS-ZIS-0.3 SIS-ZIS-0.4 SIS-ZIS-0.5	Composites based on $ZnIn_2S_4$ and $SnIn_4S_8$, number shows ½ mmol of added tin chloride during the preparation stage	10 vol.% triethanolamine	0.61 0.76 1.00 0.85 0.67	Pt, AgCl|Ag|Cl^-	0.1 M Na_2SO_4	0.0048 0.0080 0.0094 0.0083 0.0072	Xe lamp, λ ≥ 400 nm	404±73 302±54 339±61 329±59 297±53	[69]
5	CdS CdS@Ti_3C_2-5 CdS@Ti_3C_2-10 CdS@Ti_3C_2-15 CdS@Ti_3C_2-20 CdS@Ti_3C_2-25 CdS@Ti_3C_2-50 CdS@Ti_3C_2-100	CdS with different amount of deposited titanium carbide	20 vol.% methanol	0.25 0.48 0.67 1.07 0.90 0.88 0.50 0.22	Pt, AgCl|Ag|Cl^-	0.5 M Na_2SO_4	0.005 0.009 0.010 0.017 0.0095 0.009 0.0046 0.0025	Xe lamp	0.16±0.03 0.17±0.02 0.21±0.03 0.20±0.03 0.30±0.04 0.31±0.04 0.35±0.05 0.28±0.04	[77]
6	1% $CoSe_2$ 2.5% $CoSe_2$ 5% $CoSe_2$ 7.5% $CoSe_2$ 10% $CoSe_2$ 12.5% $CoSe_2$	$CdS_{0.95}Se_{0.05}$ with different amount of deposited $CoSe_2$	5 vol.% lactic acid	2.95 11.96 23.16 19.31 12.60 9.96	Pt, Hg|Hg_2Cl_2|Cl^-	0.5 M Na_2SO_4	0.011 0.022 0.057 0.047 0.028 0.017	Xe lamp	$(9±1)·10^2$ $(1.7±0.3)·10^3$ $(1.3±0.2)·10^3$ $(1.3±0.2)·10^3$ $(1.4±0.2)·10^3$ $(1.9±0.3)·10^3$	[47]
7	HD-TiO_2 3 h HD-TiO_2 4 h HD-TiO_2 5 h HD-TiO_2 6 h	Defected titania prepared during different time of hydrothermal treatment	20 vol.% methanol	11.1 12.7 15.0 10.0	Pt, Hg|Hg_2Cl_2|Cl^-	2 M Na_2SO_4	0.00036 0.00046 0.00056 0.00029	Xe lamp, λ ≥ 420 nm	$(10±1)·10^4$ $(9±1)·10^4$ $(9±1)·10^4$ $(11±2)·10^4$	[78]
8	PTCN/CN-1 PTCN/CN-2 PTCN/CN-3	Ti_3C_2/P-doped g-C_3N_4, obtained for different time of mixturing	20 vol.% methanol	0.19 0.28 0.21	Pt, AgCl|Ag|Cl^-	0.1 M Na_2SO_4	0.0006 0.0012 0.00077	Xe lamp, λ ≥ 420 nm	995±140 753±106 881±124	[72]
9	NiS/CdS-10 NiS/CdS-30 NiS/CdS-60 NiS/CdS-90 NiS/CdS-120	NiS/CdS, number shows time of mixturing of CdS suspension	20 vol.% lactic acid	0.75 1.75 3.80 6.24 4.67	Pt, Hg|Hg_2Cl_2|Cl^-	No information	1.0 1.5 2.8 5.9 4.0	Xe lamp, λ ≥ 420 nm	2.4±0.5 3.7±0.8 4.3±0.9 3.4±0.7 3.7±0.8	[79]
10	CBT-30 CBT-50 CBT-70 CBT-100	CdS/TiO_2,number shows water share in water-alcohol solution put into the autoclave	0.5 M Na_2S/Na_2SO_3	2.07 3.57 2.67 1.68	Pt, AgCl|Ag|Cl^-	0.5 M Na_2S/Na_2SO_3	3.0 4.3 3.5 2.6	Xe lamp	2.2±0.3 2.7±0.4 2.4±0.3 2.1±0.3	[68]

DOI: 10.15826/chimtech.2023.10.2.03

Table 7 Verifying the possibility of using Q1' as the similarity criterion for the series of samples with different electrolytes and their concentration.

No.	Photocatalyst	Sacrificial agent	Hydrogen production rate (μmol/min)	Counter and reference electrodes	Electrolyte	Current density (mA/cm²)	Light source	Q1'	Ref
1	$CuFe_{1.6}Mn_{0.4}O_4$	Na_2S	3.39	Pt, AgCl|Ag|Cl^-	0.1 M Na_2SO_4	0.090	Xe lamp	121±17	[80]
	$CuFe_{1.2}Mn_{0.8}O_4$		3.57			0.018		635±90	
	$CuFe_{0.8}Mn_{1.2}O_4$		3.62			0.065		178±25	
	$CuFe_{1.6}Mn_{0.4}O_4$	Na_2SO_3	0.80			0.090		29±4	
	$CuFe_{1.2}Mn_{0.8}O_4$		3.57			0.018		635±90	
	$CuFe_{0.8}Mn_{1.2}O_4$		1.56			0.065		77±11	
	$CuFe_{1.6}Mn_{0.4}O_4$	Oxalic acid	0.54			0.090		19±3	
	$CuFe_{1.2}Mn_{0.8}O_4$		0.58			0.018		103±15	
	$CuFe_{0.8}Mn_{1.2}O_4$		5.8			0.065		286±40	
2	$Cd_{0.8}Zn_{0.2}S$	20 vol.% C_2H_5OH, 0.1 M NaOH	0.04	Cu_2S/brass	20 vol.% C_2H_5OH, 0.1 M NaOH	0.008	Xe lamp	16±2	[81]
	1% CuS/ $Cd_{0.8}Zn_{0.2}S$		0.01			0.015		2.1±0.3	
	$Cd_{0.8}Zn_{0.2}S$	0.1 M Na_2S	0.10		0.1 M Na_2S	0.082		3.9±0.6	
	1% CuS/ $Cd_{0.8}Zn_{0.2}S$		0.35			0.1		11±2	
	$Cd_{0.8}Zn_{0.2}S$	0.1 M Na_2S + 0.1 M Na_2SO_3	0.59		0.1 M Na_2S + 0.1 M Na_2SO_3	0.259		7±1	
	1% CuS/ $Cd_{0.8}Zn_{0.2}S$		0.79			0.837		3.0±0.4	
	$Cd_{0.8}Zn_{0.2}S$	0.02 M Na_2S, 0.1 M Na_2SO_3	0.18		0.02 M Na_2S, 0.1 M Na_2SO_3	0.033		17±2	
		0.05 M Na_2S, 0.1 M Na_2SO_3	0.35		0.05 M Na_2S, 0.1 M Na_2SO_3	0.168		7±1	
		0.2 M Na_2S, 0.1 M Na_2SO_3	0.82		0.2 M Na_2S, 0.1 M Na_2SO_3	0.184		14±2	
		0.3 M Na_2S, 0.1 M Na_2SO_3	0.97		0.3 M Na_2S, 0.1 M Na_2SO_3	0.297		10±2	
		0.4 M Na_2S, 0.1 M Na_2SO_3	1.15		0.4 M Na_2S, 0.1 M Na_2SO_3	0.240		15±2	
		0.1 M Na_2S, 0.02 M Na_2SO_3	0.38		0.1 M Na_2S, 0.02 M Na_2SO_3	0.125		10±1	
		0.1 M Na_2S, 0.05 M Na_2SO_3	0.54		0.1 M Na_2S, 0.05 M Na_2SO_3	0.183		9±1	
		0.1 M Na_2S, 0.2 M Na_2SO_3	0.47		0.1 M Na_2S, 0.2 M Na_2SO_3	0.211		7±1	
		0.1 M Na_2S, 0.3 M Na_2SO_3	0.41		0.1 M Na_2S, 0.3 M Na_2SO_3	0.184		7±1	
	1% CuS/ $Cd_{0.8}Zn_{0.2}S$	0.02 M Na_2S, 0.1 M Na_2SO_3	0.36		0.02 M Na_2S, 0.1 M Na_2SO_3	0.219		5.3±0.7	
		0.05 M Na_2S, 0.1 M Na_2SO_3	0.62		0.05 M Na_2S, 0.1 M Na_2SO_3	0.461		4.3±0.6	
		0.2 M Na_2S, 0.1 M Na_2SO_3	0.89		0.2 M Na_2S, 0.1 M Na_2SO_3	0.727		3.9±0.6	
		0.3 M Na_2S, 0.1 M Na_2SO_3	0.83		0.3 M Na_2S, 0.1 M Na_2SO_3	0.624		4.3±0.6	
		0.4 M Na_2S, 0.1 M Na_2SO_3	0.88		0.4 M Na_2S, 0.1 M Na_2SO_3	0.444		6.3±0.9	
		0.1 M Na_2S, 0.02 M Na_2SO_3	0.48		0.1 M Na_2S, 0.02 M Na_2SO_3	0.192		8±1	
		0.1 M Na_2S, 0.05 M Na_2SO_3	0.59		0.1 M Na_2S, 0.05 M Na_2SO_3	0.424		4.5±0.6	
		0.1 M Na_2S, 0.2 M Na_2SO_3	0.62		0.1 M Na_2S, 0.2 M Na_2SO_3	0.718		2.8±0.4	
		0.1 M Na_2S, 0.3 M Na_2SO_3	0.44		0.1 M Na_2S, 0.3 M Na_2SO_3	0.605		2.3±0.3	

DOI: 10.15826/chimtech.2023.10.2.03

Copper loaded on polyaniline showed a higher catalytic activity (24% greater than 2.5% Cu/BN). The composite photocatalysts based on copper, bohrium nitride, and polyaniline were the most active in this set. Figure 2 demonstrates the criteria Q_1' and Q_3' calculated for all samples. In this particular case, the parameter values are the same and can be considered the similarity criteria.

In [57] nickel-cobalt double layered hydroxide photocatalysts were studied. Another discussed object was cobalt oxide. Because of chemical composition similarities, the ratio between the numbers of electrons used to the photocatalytic hydrogen evolution divided and those taking part in the photocurrent generation was the same and equaled 0.7 and 0.9 for cobalt oxide and double layered hydroxides, respectively. The formation of the composite catalyst from these components allowed enhancing the photocatalytic hydrogen production by 5–8 times and increasing the photocurrent generation by 4–7 times compared with pristine compounds [57]. The Q_1' criterion retained the value obtained for nickel-cobalt double layered hydroxides whose surface was modified with CoO by the hydrothermal method. The same result was reached for zinc sulfide and one deposited with polydopamine described in [58]. Such modification allowed improving the target characteristics of the photocatalysts and photoelectrodes and keeping Q_1' within experimental error. The same behavior was demonstrated for metal-organic frameworks discussed in [59]. The deposition of 5% NiS led to the increase of the photocatalytic hydrogen production rate from aqueous solution of triethanolamine by 4.5 times, while the generated current density was enhanced by 3.5 times. The ratio of the electrons occurring in these processes remained the same. In [53] $ZnIn_2S_4$ was deposited on NH_2-UiO-66 and decarboxylated NH_2-UiO-66. The Q_1' criteria differed for pristine samples, while Q_1' was the same for the composite photocatalysts and $ZnIn_2S_4$. Finally, the same values of Q_1' were calculated for graphitic carbon nitride modified with platinum or platinum oxide [60]. The same behavior was found for CdS whose surface was modified with carbon quantum dots. The photocatalytic hydrogen production rate and the photocurrent density doubled in these systems while the Q_1' criterion was the same within the experimental errors [61].

The contrary trend was characterized for other systems described earlier. For instance, in [62] the photocatalysts based on silicon dioxide and the co-catalyst modified with red phosphorous were studied. The replacement of platinum co-catalyst with cobalt phosphide led to the growth of the catalytic activity and the ratio of the number of electrons used for the photocatalytic hydrogen evolution to the number of electrons taking part in the photocurrent generation. Probably, different co-catalysts significantly changed the rate constants of the corresponding processes, which leads to the observed changes in the system. The same behavior was found in the case of CdS whose catalytic properties were improved with deposition of 20 wt.% WN [63]. The co-catalyst addition allowed enhancing the hydrogen production rate by 9.3 times while the photocurrent generation was increased by 4.2 times, the Q_1' criterion grew by 2.2 times. In [64] researches discussed titanium dioxide prepared by the template method. The reduction of titania by sodium borohydride led to an increase in the reaction rate of hydrogen photoproduction from aqueous methanol solution by 20%; the studied ratio of the electrons occurring in the photocatalytic and the photovoltaic properties did not change in this case. Additionally, the authors improved the target characteristics by the deposition of polyaniline and polyaniline and silver on the photocatalyst surface. Such modifications favored the photocatalytic hydrogen production; however, the Q_1' criteria were different for the obtained samples as shown in Figure 3.

The authors of [65] compared the target properties of graphitic carbon nitride prepared by different methods such as thermal polymerization and template synthesis. At whole, the template method allowed getting more active samples; the ratio between the number of electrons used for the photocatalytic hydrogen evolution and the number of electrons taking part in the photocurrent generation was the same within experimental errors. The subsequent modification of carbon nitride with cobalt oxide changed the electronic properties of the semiconductor, improved the target characteristics of the photocatalytic and photovoltaic phenomena; the Q_1' parameter was also changed.

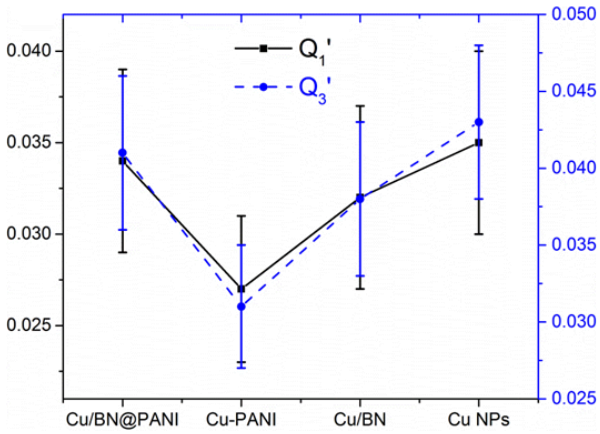

Figure 2 Parameters Q_1' and Q_3' calculated for the Cu-containing photocatalysts described in [56].

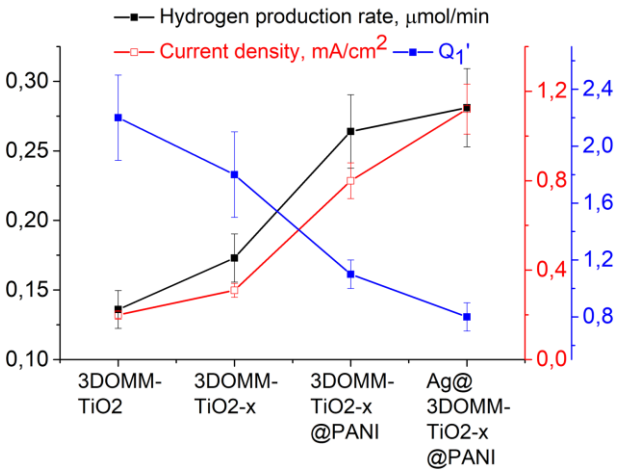

Figure 3 The catalytic activities, current densities, and parameters Q_1' calculated for the titania-based photocatalysts discussed in [64].

 DOI: 10.15826/chimtech.2023.10.2.03

The illustration of the significant change in the parameter Q_1' was the work [66] in which molybdenum phosphide (25 wt.%) was deposited on the surface of indium sulfide. It caused the increase in the rate of the photocatalytic hydrogen production from lactic acid, the photocurrent generation, and Q_1' value by 160, 2.9, and 53 times, respectively. The same result was found for CdS modified with 11 wt.% iron phosphide, where the co-catalyst addition led to the growth of the reaction rate, the photocurrent generation, and Q_1' by 79, 14, and 5.7 times, respectively [67].

In [68] titania and the composite samples based on titania and cadmium sulfide were tested in 0.5 M Na_2S/Na_2SO_3. The composite photocatalysts were more active under visible light than pristine titania or cadmium sulfide due to the heterojunction formation. Perhaps, the heterojunctions changed the number of electrons taking part in the photocatalytic reaction and photocurrent generation, and its ratio defined by Q_1'. In [69] reduced graphene oxide deposited on $La_2Ti_2O_7$, $La_2Ti_2O_7$ deposited on nickel-iron-double layered hydroxides, the composite material consisting of graphene oxide, nickel-iron-double layered hydroxides, and $La_2Ti_2O_7$. Figure 4 reveals that as for CdS/TiO_2, the reaction rates, the current density, and Q_1' differed for the composite photocatalysts.

Thus, in the case of combining materials of different composition, the parameter Q_1' can either preserve the constant value of the pristine material or change. Probably, the specific values of the parameter are related to the balance of various rate constants that described the processes of electron-hole generation, their transfer and recombination. Generally, the condition of physical similarity is not met for the catalysts having different chemical nature. However, in several cases, we can talk about partial similarity.

Doping. The authors [70] studied the doping of cadmium sulfide with molybdenum. The introduction of 25 wt.% of MoS_2 led to an increase in the reaction rate and the photocurrent generation, while the ratio of the number of electrons used for the photocatalytic hydrogen evolution to the number of electrons taking part in the photoelectrochemical processes was the same. The introduction of Al to zinc oxide (up to 5 wt.%) improved the target characteristics, while the Q_1' criteria were the same within experimental error [71] as shown in Figure 5.

The researchers studied doped graphitic carbon nitride. In [72] phosphorous was used as the dopant; its introduction in the structure allowed improving the target characteristics; however, the ratio of electrons did not remain constant and grew during the doping. Probably, this behavior was related to reaction rate constants of the processes occurring when P was introduced into the electronic structure of carbon nitride. The authors [73] discussed carbon nitride doped by B and Cs simultaneously for different forms such as nanoparticles and nanosheets. It should be noted that the introduction of these elements into the structure allowed improving both the photocatalytic and photovoltaic characteristics of the materials. However, Figure 6 shows that the ratio of the number of electrons used to the photocatalytic hydrogen evolution to the number of electrons taking part in the photoelectrochemical processes was the same for the nanoparticles and differed for the nanosheets.

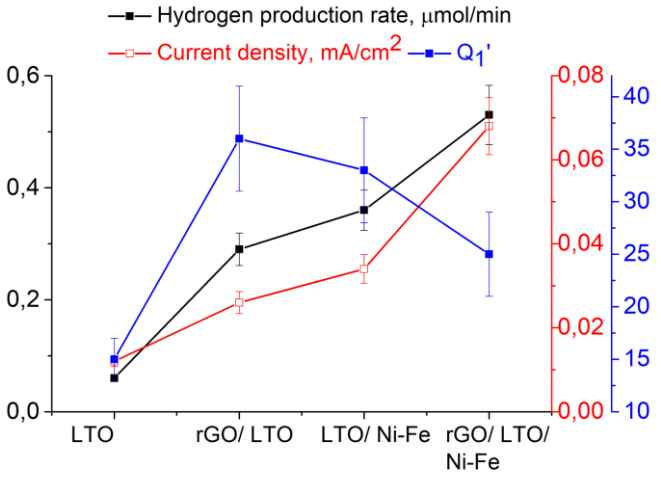

Figure 4 The catalytic activities, current densities, and parameters Q_1' calculated for the LTO-based samples mentioned in [69].

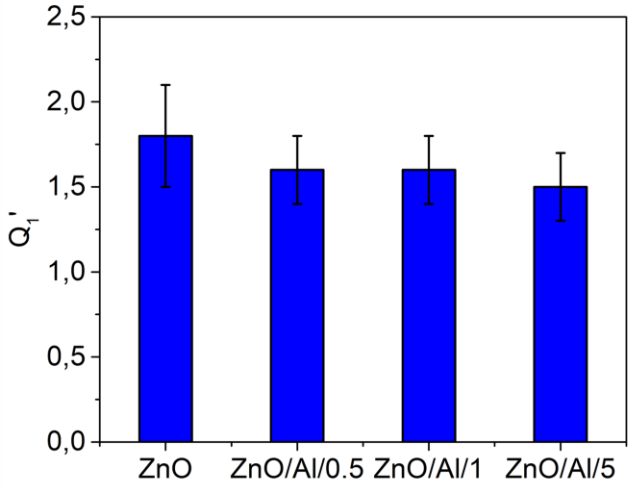

Figure 5 The Q_1' parameter calculated for the Al-doped ZnO samples described in [71].

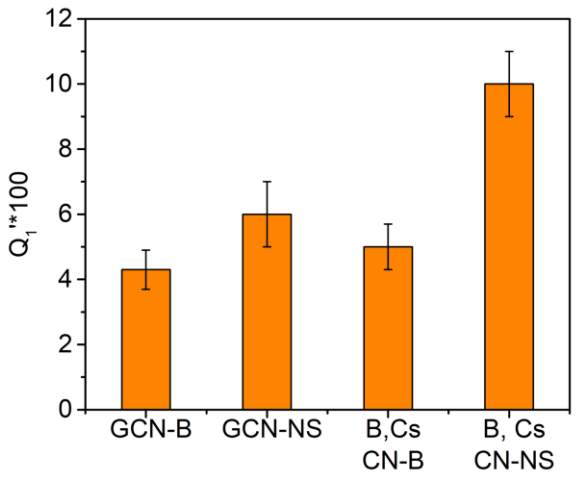

Figure 6 The Q_1' parameter calculated for the samples based on carbon nitride (GCN) discussed in [73]. NS denotes nanosheets.

 DOI: 10.15826/chimtech.2023.10.2.03

In [74] the effect of benzoquinone on the target characteristics of carbon nitride obtained by crosslinking polymer chains of carbon nitride was described. In this case, the change in the electronic properties was similar to ones occurring during doping because the additional impurity level was formed in the electronic structure, which improved charge separation. The appearance of this level contributed to the increase in the reaction rate and photocurrent generation by a factor of 2.3 while the Q_1' was the same and equaled 8 [74]. Thus, in the case of doping, the parameter Q1' can both keep constant during the transition between samples and change.

3.3. Samples in which weight ratios of components were changed

Table 6 contains the data obtained for the samples during whose preparation the weight ratio of components or reaction time were changed. This case was considered on the example of ten series of samples with different chemical nature. In [62] the composite photocatalysts based on cobalt phosphide deposited on the silica surface for different time periods (the time in hours is written in the sample label in Table 6) with subsequent deposition of red phosphorous were studied. The ratio of electron amount used in the target processes was the same and equaled ~40 for all samples. In the case of the samples based on cadmium sulfide and molybdenum sulfide [75], the same result was found; increasing MoS_2 amount from 6 to 25 wt.% led to the halving of the photocatalytic hydrogen production rate and the photocurrent density, while the Q_1' criterion remained constant. The authors [76] discussed the composite photocatalysts consisting of lanthanum vanadate and graphitic carbon nitride; the photocatalytic and photovoltaic properties were studied for samples with w($LaVO_4$) from 0 to 25%. The changes in the target properties had a bell-shaped character, while their ratio was the same within the experimental error. For the sample with 25 wt.% $LaVO_4$, a slight decrease in this parameter was observed. Possibly, it was related to the change in the geometric structure of the catalyst. The excess (relative to the optimal) content of lanthanum vanadate was associated with the location of particles that block the photocatalyst's active centers. During the transition between catalysts of different geometric structures, the conditions of geometric and/or physical similarity were violated, as a result of which the potential similarity criteria, as seen in Figure 7, will not be preserved.

In [69] the composite photocatalysts based on $ZnIn_2S_4$ and $SnIn_4S_8$ were described. The dependences of the hydrogen production rate and the photocurrent density on the catalyst composition went through a maximum. The ratio of the electron number used in the target processes remained the same for the transition from one sample to another and was 300–400 within experimental error. Another situation was found for CdS whose surface was modified with titanium carbide (Figure 8) [77]. The dependences of the reaction rate and the current density on the titanium carbide content was domed, the maximum values were observed for 15 wt.% of titanium carbide. However, the Q_1' criteria were the same values within experimental error for the samples with 15% Ti_3C_2 (Q_1' ~ 0.16) and greater than 15% Ti_3C_2 (Q_1' ~ 0.28). Such difference may be due to the textural characteristics of the samples or the number of interfacial contacts; the increase in the Ti_3C_2 content led to the growth of the interfacial contacts and the surface area. After achieving the optimal structure of CDs@Ti_3C_2-15, the number of contacts between titanium carbide and cadmium sulfide decreased, and the surface area and pore volume also declined. Thus, in this case, the appearance of two groups of samples with different similarity criteria was connected with the change in their geometric structure; the theory of similarity within each group was fulfilled.

In [47] the photocatalysts based on the solid solution of cadmium sulfide and cadmium selenide with deposited cobalt selenide were studied. As for other deposited photocatalysts, the dependences of the hydrogen production rate and the photocurrent density on the co-catalyst content had a wide peak shape, as shown in Figure 9.

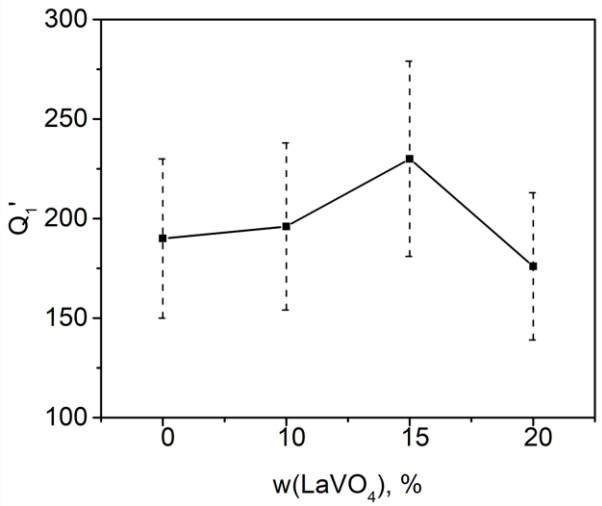

Figure 7 The Q_1' parameter calculated for the photocatalysts $LaVO_4$/CdS with different $LaVO_4$ content (based on data described in [76]).

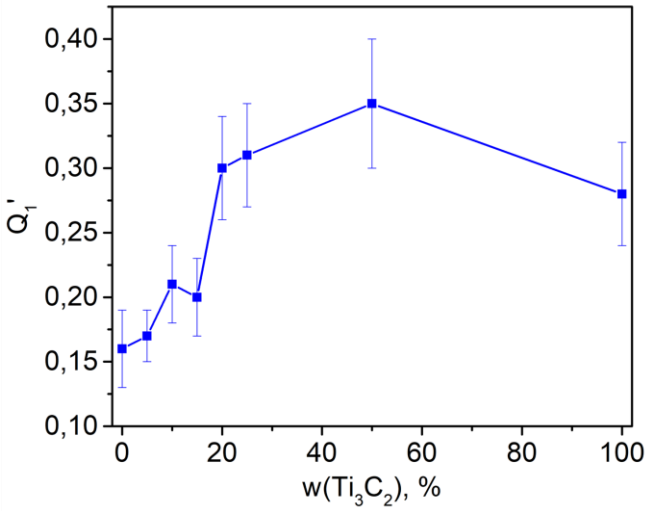

Figure 8 The dependence of Q_1' on the co-catalyst content for the composites CdS@Ti_3C_2 discussed in [77].

 DOI: 10.15826/chimtech.2023.10.2.03

The ratio of the target characteristics denoted as Q_1' was the same within experimental error for all samples, excluding one with 1% $CoSe_2$. Unfortunately, it was difficult to determine the reasons for such deviation due to the lack of information about the texture and structure of the mentioned sample.

In [78] the defect-containing titania prepared by the hydrothermal treatment at 3–6 h was studied. The hydrothermal treatment allowed obtaining the samples with oxygen vacancies whose amount impacted the hydrogen production and the photocurrent generation. The ratio of the electros taking part in the target processes was the same for all samples. The Q_1' criterion may serve as the similarity criterion in case of the composite materials based on graphitic carbon nitride doped by P and titanium carbide; the catalyst components were mixed at different time [72]. In [79] CdS with deposited NiS was described, and the crystallization time of CdS was varied. Figure 10 showed that for this set of samples the Q_1' value remained constant, excluding the first sample. This was probably due to the low crystallization time and the resulting deviations in the structure of the catalyst in relation to other samples.

Another way of changing the synthesis conditions, indirectly related to the change in the mass ratios of the catalyst components, was the variation of the solvent composition during the synthesis [68]. The number of electrons occurring in the photocatalytic hydrogen production divided by the number of electrons taking part in the photocurrent generation was the same for transition between the samples in this set.

To sum up, if the conditions of geometric and physical similarity are fulfilled, the parameter Q_1' revealing the ratio of electrons taking part in the target processes can act as the similarity criterion revealing the relation between the efficiencies of the photocatalytic hydrogen production and the photocurrent generation for different samples.

3.4. Studying photocatalytic and photovoltaic properties in different electrolytes

Table 7 showed the data obtained over samples in different electrolytes [80, 81]. Unfortunately, little attention has been paid to the study of this issue in the literature. In [80] the authors described photocatalytic processes of the solid solution of copper oxide, iron oxide, and manganese oxide in aqueous solutions of sodium sulfide, sodium sulfite, and oxalic acid. For comparison, the photocurrent generation was carried out in 0.1 M Na_2SO_4 solution. In case of inorganic salts, the dependence of hydrogen production rate on the solid solution composition went through a maximum, while for the photocurrent generation this dependence went through a minimum. In case of oxalic acid, the reaction rate increased for the discussed samples. This behavior of the target characteristics was connected with electrolyte nature and different transformations in various media. So, it was difficult to identify any features for the ratio of electrons taking part in target processes.

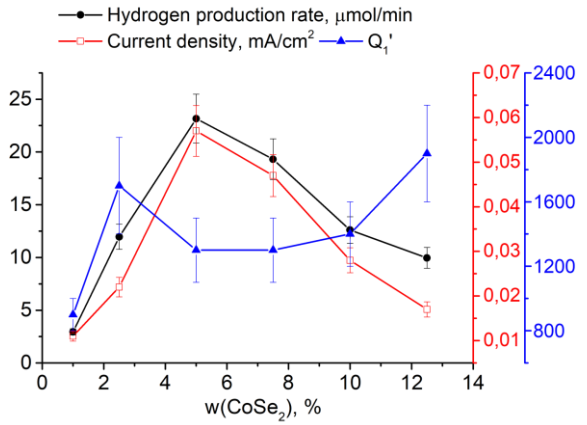

Figure 9 The dependences of target values and Q_1' on the $CoSe_2$ content for the photocatalysts $CoSe_2/CdS_{0.95}Se_{0.05}$ described in [47].

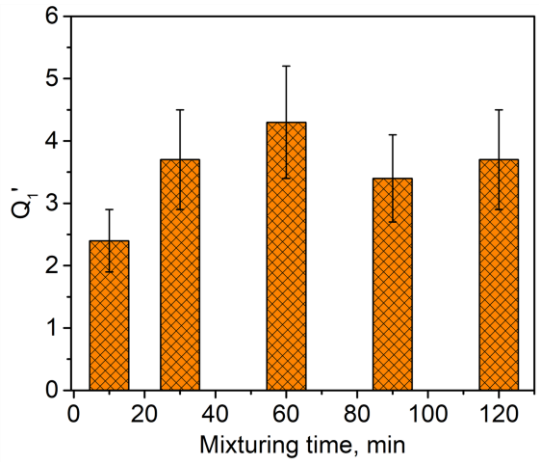

Figure 10 The dependence of Q_1' on the mixturing time of CdS suspension obtained for NiS/CdS samples discussed in [79].

The Q_1' criterion did not remain the same for transition between different solutions and catalysts.The solutions of distinct nature or concentration possessed different properties such as dielectric constant, density, viscosity, etc., that impacted the charge transfer and current generation. Therefore, the condition of physical similarity of the discussed systems was not fulfilled; the transition between different solutions for the same sample cannot be considered using the similarity theory. The same conclusion may be made based on the results described in [81]. In that paper the photocatalytic and photovoltaic properties were studied in 20 vol.% C_2H_5OH, 0.1 M NaOH, 0.1 M Na_2S, 0.1 M Na_2S + 0.1 M Na_2SO_3. As in the previous case, the features of the photocatalytic hydrogen production and photocurrent generation were different in various media.

Figures 11 and 12 reveal that when the ratio of salts in the solution varied, the dependences of the target characteristics on the composition of the electrolyte remained at a qualitative level. However, the Q_1' criterion changed from 7 to 17 and from 2 to 8 for $Cd_{0.8}Zn_{0.2}S$ and 1% $CuS/Cd_{0.8}Zn_{0.2}S$, respectively. Thus, in terms of the similarity theory, consideration of the question of transferring the dependence of photocatalytic hydrogen production on photovoltaic parameters was incorrect.

 DOI: 10.15826/chimtech.2023.10.2.03

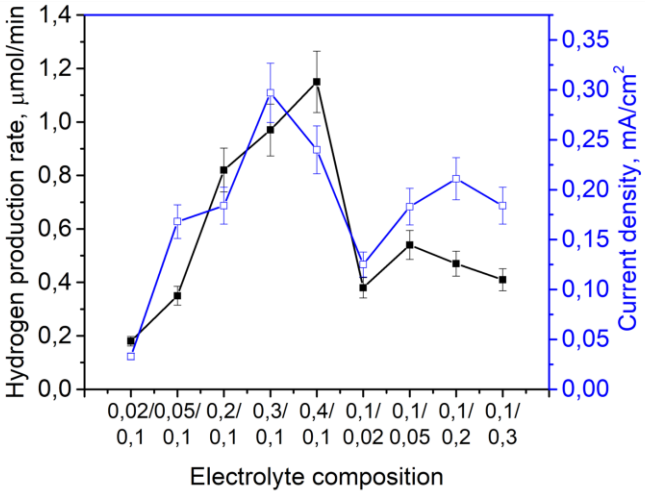

Figure 11 The dependence of the target characteristics of $Cd_{0.8}Zn_{0.2}S$ measured in Na_2S/Na_2SO_3 [81]. The electrolyte composition was labeled as a/b, where a is the concentration of Na_2S, M, b is the concentration of Na_2SO_3, M.

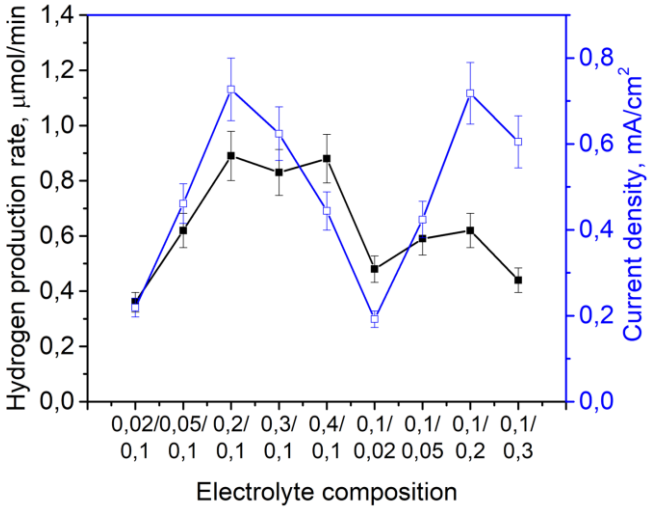

Figure 12 The dependence of the target characteristics of 1% $CuS/Cd_{0.8}Zn_{0.2}S$ measured in Na_2S/Na_2SO_3 [81]. The electrolyte composition was labeled as a/b, where a is the concentration of Na_2S, M, b is the concentration of Na_2SO_3, M.

4. Limitations

The topic of the transfer from the photocatalytic reaction to the photocurrent generation has some promising research directions such as the calculation and verification Q_2 and Q_4, getting more information about rate constants and interpretation of the criterion values, discussing other photocatalytic reactions besides hydrogen production, etc.

5. Conclusions

The photocatalytic hydrogen production and photocurrent generation in the photoelectrochemical cell are analogous phenomena; so, one can use the similarity theory for their description. Using dimension theory, two parameters which could potentially act as the similarity criteria revealing relation between efficiencies of the photocatalytic hydrogen evolution and the photocurrent generation were obtained. The first parameter is the ratio of the number of electrons involved in the photocatalytic hydrogen production to the number of electrons taking part in the photocurrent generation. The latter value takes into account the energy aspects of converting light energy into chemical bond and electrical energy. The analysis of the literature data allowed verifying the first criterion and showed that the ratio of the number of electrons did act as a similarity criterion if the conditions of geometric and physical similarity were fulfilled. In practice, this means that the ratio between the quantitative indicators of the photocatalytic hydrogen production and photocurrent generation remained constant in the case of the same chemical nature of the samples, for example, in the set with different ratios of the catalyst components, with the same morphology and texture, or in the case of the solid solutions formation with a similar composition. Generally, if the photocatalyst modification by chemical compounds changes the physicochemical properties of samples, such cases, as well as data analysis in various media, cannot be considered in the similarity theory and should be studied individually.

• Supplementary materials

No supplementary materials are available.

• Funding

This work was supported by the Ministry of Science and Higher Education of the Russian Federation within the governmental order for Boreskov Institute of Catalysis, project no. AAAA-A21-121011390009-1.

• Acknowledgments

None.

• Author contributions

Conceptualization: E.A.K., D.V.M.
Data curation: D.V.M.
Formal Analysis: D.V.M.
Funding acquisition: E.A.K.
Investigation: D.V.M.
Methodology: D.V.M.
Project administration: E.A.K.
Resources: E.A.K.
Software: E.A.K.
Supervision: E.A.K.,D.V.M.
Validation: D.V.M.,E.A.K.
Visualization: D.V.M.
Writing – original draft: D.V.M.
Writing – review & editing: E.A.K.,D.V.M.

• Conflict of interest

The authors declare no conflict of interest.

 DOI: 10.15826/chimtech.2023.10.2.03

• Additional information

Author IDs:

Dina V. Markovskaya, Scopus ID 55895307200;

Ekaterina A. Kozlova, Scopus ID 12244601300.

Website:

Boreskov Institute of Catalysis, https://catalysis.ru.

References

1. Turner JA. Sustainable hydrogen production. Sci. 2004;305(5686):972–974. doi:10.1126/science.1103197
2. Fujishima A, Honda K. Electrochemical photolysis of water at a semiconductor electrode. Nat. 1972;238:37–38. doi:10.1038/238037a0
3. Vorontsov AV, Kozlova EA, Besov AS, Kozlov DV, Kiselev SA, Safatov AS. Photocatalysis: light energy conversion for the oxidation, disinfection, and decomposition of water. Kin Cat. 2010;51(6):801–808. doi:10.1134/S0023158410060042
4. Tomboc GM, Gadisa BT, Joo J, Kim H, Lee K. Hollow structured metal sulfides for photocatalytic hydrogen generation. ChemNanoChem. 2020;6(6):850–869. doi:10.1002/cnma.202000125
5. Stolarczyk JK, Bhattacharyya S, Polavarapu L, Feldmann J. Challenges and prospects in solar water splitting and CO_2 reduction with inorganic and hybrid nanostructures. ACS Catal. 2018;8(4):3602–3635. doi:10.1021/acscatal.8b00791
6. Li X, Wang W, Dong F, Zhang Z, Han L, Luo X, Huang J, Feng Z, Chen Z, Jia G, Zhang T. Recent advances in noncontact external-field-assisted photocatalysis: from fundamentals to applications. ACS Catal. 2021;11(8):4739–4769. doi:10.1021/acscatal.0c05354
7. Krjukov AI, Strojuk AL, Kuchmij SYa, Pohodenko VD. Nanofotokataliz [Nanophotocatalysis]. Kiev: Akademperiodika; 2013. 618 p. Russian.
8. Cao S, Wang C-J, Fu W-F, Chen Y. Metal phosphides as co-catalysts for photocatalytic and photoelectrocatalytic water splitting. ChemSusChem. 2017;10(22):4306–4323. doi:10.1002/cssc.201701450
9. Carp O, Huisman CL, Reller A. Photoinduced reactivity of titanium dioxide. Prog Solid State Ch. 2004;32:33–177. doi:10.1016/j.progsolidstchem.2004.08.001
10. Frank-Kamenetsky DA. Osnovy makrokinetiki. Diffuziya i teploperedacha v himicheskoj kinetike [Fundamentals of macrokinetics. Diffusion and heat transfer in chemical kinetics]. Dolgoprudny: Izdatel'skij dom "Intellekt"; 2008. 408 p. Russian.
11. Sedov LI. Metody podobiya i razmernosti v mehanike [Similarity and dimensionality methods in mechanics]. Moscow: Nauka; 1977. 440 p. Russian.
12. Liu Z, Yu Y, Zhu X, Fang J, Xu W, Hu X, Li R, Yao L, Qin J, Fang Z. Semiconductor heterojunctions for photocatalytic hydrogen production and Cr(VI) reduction: a review. Mater Res Bull. 2022;147:111636. doi:10.1016/j.materresbull.2021.111636
13. Ismael M. Latest progress on the key operating parameters affecting the photocatalytic activity of TiO2-based photocatalysts for hydrogen fuel production: a comprehensive review. Fuel. 2021;303:121207. doi:10.1016/j.fuel.2021.121207
14. Vyas Y, Chundawat P, Dharmendra D, Punjabi PB, Ameta C. Review on hydrogen production photocatalytically using carbon quantum dots: future fuel. Int J Hydrog Energy. 2021;46(75):37208–37241. doi:10.1016/j.ijhydene.2021.09.004
15. Kozlova EA, Lyulyukin MN, Markovskaya DV, Selishchev DS, Cherepanova SV, Kozlov DV. Synthesis of $Cd_{1-x}Zn_xS$ photocatalysts for gas-phase CO_2 reduction under visible light. Photoch Photobio Sci. 2019;18(4):871–877. doi:10.1039/c8pp00332g
16. Tasleem S, Tahir M. Recent progress in structural development and band engineering of perovskites materials for photocatalytic solar hydrogen production: a review. Int J Hydrog Energy. 2020;45(38):19078–19111. doi:10.1016/j.ijhydene.2020.05.090
17. Al-Ahmed A. Photocatalytic properties of graphitic carbon nitrides (g-C_3N_4) for sustainable green hydrogen production: recent advancement. Fuel. 2022;316:123381. doi:10.1016/j.fuel.2022.123381
18. Singla S, Sharma S, Basu S, Shetti NP, Aminabhavi TM. Photocatalytic water splitting hydrogen production via environmental benign carbon based nanomaterials. Int. J. Hydrogen Energy. 2021;46(68):33696–33717. doi:10.1016/j.ijhydene.2021.07.187
19. Lv Y, Chen P, Foo JJ, Zhang J, Qian W, Chen C, Ong W-J. Dimensionality-dependent MoS2 toward efficient photocatalytic hydrogen evolution: from synthesis to modifications in doping, surface and heterojunction engineering. Mater Today Nano. 2022;18:10019. doi:10.1016/j.mtnano.2022.100191
20. Kozlova EA, Parmon VN. Heterogeneous semiconductor photocatalysts for hydrogen production from aqueous solutions of electron donors. Russ Chem Rev. 2017;86(9):870–906. doi:10.1070/RCR4739
21. Braslavsky SE, Braun AM, Cassano AE, Emeline AV, Litter MI, Palmisano L, Parmon VN, Serpone N. Glossary of terms used in photocatalysis and radiation catalysis (IUPAC Recommendations 2011). Pure Appl Chem. 2011;83(4):931–1014. doi:10.1351/PAC-REC-09-09-36
22. Lakhera SK, Rajan A, Rugma TP, Bernaurdshaw N. A review on particulate photocatalytic hydrogen production system: Progress made in achieving high energy conversion efficiency and key challenges ahead. Renew Sustain Ener Rev. 2021;152:11169. doi:10.1016/j.rser.2021.111694
23. Boreskov GK. Geterogennyj kataliz [Heterogeneous catalysis]. Moscow: Nauka; 1986. 304 p. Russian.
24. Nakamura A, Ota Y, Koike K, Hidaka Y, Nishioka K, Sugiyama M, Fujii K. A 24.4% solar to hydrogen energy conversion efficiency by combining concentrator photovoltaic modules and electrochemical cells. Appl Phys Expess. 2015;8:107101. doi:10.7567/apex.8.107101
25. Ziegenbalg D, Pannwitz A, Rau S, Dietzek-Ivanšić B, Streb C. Comparative evaluation of light-driven catalysis: a framework for standardized reporting of data. Angew Chem-Ger Edit. 2022;61(28):e202114106. doi:10.1002/anie.202114106
26. Chen S, Liu T, Zheng Z, Ishaq M, Liang G, Fan P, Chen T, Tang J. Recent progress and perspectives on Sb_2Se_3-based photocathodes for solar hydrogen production via photoelectrochemical water splitting. J Energy Chem. 2022;67:508–523. doi:10.1016/j.jechem.2021.08.062
27. Lewerenz HJ. Micro- and nanotopographies for photoelectrochemical energy conversion. I: The photovoltaic mode. Electrochim Acta. 2011;56(28):10713–10725. doi:10.1016/j.electacta.2011.05.026
28. Ahmed M, Dincer I. A review on photoelectrochemical hydrogen production systems: Challenges and future directions. Int J Hydrog Energy. 2019;44(5):2474–2507. doi:10.1016/j.ijhydene.2018.12.037
29. Esmaili H, Kowsari E, Tafreshi SS, Ramakrishna S, de Leeuw NH, Abdouss M. TiO2 nanoarrays modification by a novel Cobalt-heteroatom doped graphene complex for photoelectrochemical water splitting: An experimental and theoretical study. J Mol Liq. 2022;356:118960. doi:10.1016/j.molliq.2022.118960
30. Chavan GT, Shinde NM, Sabah FA, Patil SS, Sikora A, Prakshale VM, Kamble SS, Chaure NB, Deshmukh LP, Kim A, Jeon C-W. Chemical synthesis of $Cd_{1-x-y}Zn_xCu_yS_zSe_{1-z}$ composite thin films for photoelectrochemical solar cell. Appl Surf Sci. 2022;574:2022. doi:10.1016/j.apsusc.2021.151581
31. Chatterjee P, Ambati MSK, Chakraborty AK, Chakrabortty S, Biring S, Ramakrishna S, Wong TKS, Kumar A, Lawaniya R, Dalapati GK. Photovoltaic/photo-electrocatalysis integration

 DOI: 10.15826/chimtech.2023.10.2.03

for green hydrogen: A review. Energ Convers Manage. 2022;261:115648. doi:10.1016/j.enconman.2022.115648
32. Ikram A, Zulfequar M, Satsangi VR. Role and prospects of green quantum dots in photoelectrochemical hydrogen generation: A review. Int J Hydrog Energy. 2022;47(22):11472–11491. doi:10.1016/j.ijhydene.2022.01.187
33. Lee SY, Oh J-Y, Patil RP, Kim M, Jang JS, Jin H, Kim S, Lee HJ. A general guide for adsorption of cadmium sulfide (CdS) quantum dots by successive ionic layer adsorption and reaction (SILAR) for efficient CdS-sensitized photoelectrochemical cells. Appl Surf Sci. 2022;589:152898. doi:10.1016/j.apsusc.2022.152898
34. Hogerwaard J, Dincer I, Naterer GF. Experimental investigation and optimization of integrated photovoltaic and photoelectrochemical hydrogen generation. Energ Convers Manage. 2020;207:112541. doi:10.1016/j.enconman.2020.112541
35. Shiyani T, Mahapatra SK, Banerjee I. Basil sensitized ZnO photoelectrochemical cell for solar energy conversion. Mater Today-Proc. 2020;32(3):412–416. doi:10.1016/j.matpr.2020.02.089
36. Shang J, Gao Y, Chen H, Wang X. Top-down fabrication of bromine doped Bi_2O_3 nanowires with efficient charge separation for photoelectrochemical application. Physica B: Condensed Matter. 2020;599:412587. doi:10.1016/j.physb.2020.412587
37. Ali M, Pervaiz E, Sikandar U, Khan Y. A review on the recent developments in zirconium and carbon-based catalysts for photoelectrochemical water-splitting. Int J Hydrog Energy. 2021;46(35):18257–18283. doi:10.1016/j.ijhydene.2021.02.202
38. Knapik A, Syrek K, Kozieł M, Zaraska L. Cathodic deposition of SnO_2 layers on transparent conductive substrates and their photoelectrochemical activity. J Ind Eng Chem. 2022;111:380–388. doi:10.1016/j.jiec.2022.04.020
39. Zhang Y, Bu Y, Wang L, Ao J-P. Regulation of the photogenerated carrier transfer process during photoelectrochemical water splitting: A review. Green Energy Environ. 2021;6(4):479–495. doi:10.1016/j.gee.2020.11.007
40. Hashim ET, Abdulameer A. Temperature effect on power drop of different photovoltaic modules. J Eng. 2016;22(5):129–143. English. Available from: https://www.iasj.net/iasj/download/dfbe920adbae6455. Accessed on 08.02.2023.
41. Gurevich YuYa, Pleskov YuV. Photoelectrohimiya poluprovodnikov [Photoelectrochemistry of semiconductors]. Moscow: Nauka; 1983. 312 p. Russian.
42. Kamat PV, Tvrdy K, Baker DR, Padich JG. Beyong photovoltaics: semiconductor nanoarchitectures for liquid-junction solar cells. Chem Rev. 2010;110:6664–6688. doi:10.1021/cr100243p
43. Chen Z, Jaramillo TF, Deutsch TG, Kleiman-Shwarsctein A, Forman AJ, Gaillard N, Garland R, Takanabe K, Heske C, Sunkara M, McFarland EW, Domen K, Miller EL, Turner JA, Dinh HN. Accelerating materials development for photoelectrochemical hydrogen production: Standards for methods, definitions, and reporting protocols. J Mater Res. 2010;25:3–16. doi:10.1557/JMR.2010.0020
44. Strenk F. Peremeshivanije i apparaty s meshalkami [Mixing and devices with agitators]. Leningrad: Himiya; 1975. 384 p. Russian.
45. Antoniadou M, Daskalaki VM, Balis N, Kondarides DI, Kordulis C, Lianos P. Photocatalysis and photoelectrocatalysis using (CdS-ZnS)/TiO2 combined photocatalysts. Appl Catal B-Environm. 2011;107(1–2):188–196. doi:10.1016/j.apcatb.2011.07.013
46. Markovskaya DV, Zhurenok AV, Cherepanova SV, Kozlova EA. Solid solutions of CdS and ZnS: comparing photocatalytic activity and photocurrent generation. Appl Surf Sci Adv. 2021;4:100076. doi:10.1016/j.apsadv.2021.100076
47. Du S, Lin X, Li C, Li G, Zheng B, Liu Y, Xu H, Fang P. CoSe2 modified Se-decorated CdS nanowire Schottky heterojunctions for highly efficient photocatalytic hydrogen evolution. Chem Eng J. 2020;389:124431. doi:10.1016/j.cej.2020.124431
48. Li H, Wang Z, He Y, Meng S, Xu Y, Chen S, Fu X. Rational synthesis of MnxCd1–xS for enhanced photocatalytic H2 evolution: Effects of S precursors and the feed ratio of Mn/Cd on its structure and performance. J Colloid Interf Sci. 2019;535:469–480. doi:10.1016/j.jcis.2018.10.018
49. Zhao Y, Yang P, Li J. Fabrication of one-dimensional $Mn_xCd_{1-x}S$@D–$MoSe_yS_{2-y}$ heterostructure with enhanced visible-light photocatalytic hydrogen evolution. Int J Hydrog Energy. 2021;46(43):22422–22433. doi:10.1016/j.ijhydene.2021.04.063
50. Guo P, Zhang D, Liu X, Liu W, Wang R, Zhang Z, Qiu S. In situ self-assembly of mesoporous Zn-Cd-Mo-S quaternary metal sulfides with double heterojunction synergistic charge transfer for boosting photocatalytic hydrogen production. J Alloy Compd. 2022;921:166066. doi:10.1016/j.jallcom.2022.166066
51. Kalia R, Pushpendra, Kunchala RK, Achary SN, Naidu BS. New insights on photocatalytic hydrogen evolution of $ZnFe_{2-x}Ga_xO_4$ ($0 \leq x \leq 2$) solid solutions: Role of oxygen vacancy and ZnO segregated phase. J Alloy Compd. 2021;875:159905. doi:10.1016/j.jallcom.2021.159905
52. Ren B, Luan Q, Ma LL, Ding Y, Ma D, Cao X, Guo Y, Guan R, Chen Q. Amorphous domain induced LSPR Zn–Cr–In–S solid solution with enhanced visible photocatalytic H_2 production. Mater Chem Phys. 2022;285:126100. doi:10.1016/j.matchemphys.2022.126100
53. Zhao C, Jiang H, Liang Q, Zhou M, Zhang Y, Li Z, Xu S. NH2-UiO-66 with heterogeneous pores assists zinc indium sulfide in accelerating the photocatalytic H_2 evolution under visible-light irradiation. Sol Energy. 2020;207:599–608. doi:10.1016/j.solener.2020.07.005
54. Liu X, Wen D, Liu Z, Wei J, Bu D, Huang S. Thiocyanate-capped CdSe@$Zn_{1-X}Cd_XS$ gradient alloyed quantum dots for efficient photocatalytic hydrogen evolution. Chem Eng J. 2020;402:126178. doi:10.1016/j.cej.2020.126178
55. Huang J, Tao J, Liu G, Lu L, Tang H, Qiao G. In situ construction of 1D CdS/2D Nb2CTx MXene Schottky heterojunction for enhanced photocatalytic hydrogen production activity. Appl Surf Sci. 2022;573:151491. doi:10.1016/j.apsusc.2021.151491
56. Sk S, Tiwari A, Abraham BM, Manwar N, Perupogu V, Pal U. Constructing Cu/BN@PANI ternary heterostructure for efficient photocatalytic hydrogen generation: A combined experimental and DFT studies. Int J Hydrog Energy. 2021;46(54):27394–27408. doi:10.1016/j.ijhydene.2021.06.033
57. Wang Y, Guo S, Xin X, Zhang Y, Wang B, Tang S, Li X. Effective interface contact on the hierarchical 1D/2D CoO/NiCo-LDH heterojunction for boosting photocatalytic hydrogen evolution. Appl Surf Sci. 2021;549:149108. doi:10.1016/j.apsusc.2021.149108
58. Kim Y, Coy E, Kim H, Mrówczyński R, Torruella P, Jeong D-W, Choi KS, Jang JH, Song MY, Jang D-J, Peiro F, Jurga S, Kim HJ. Efficient photocatalytic production of hydrogen by exploiting the polydopamine-semiconductor interface. Appl Catal B-Environ. 2021;280:119423. doi:10.1016/j.apcatb.2020.119423
59. Xu G, Lin X, Tong Y, Du H, Gu L, Yuan Y. UiO-66 MOFs as electron transport channel to short circuit dye photosensitizer and NiS_2 co-catalyst for increased hydrogen generation. Mater Lett. 2019;255:126593. doi:10.1016/j.matlet.2019.126593
60. Wang C, Fan H, Ren X, Wen Y, Wang W. Highly dispersed PtO nanodots as efficient co-catalyst for photocatalytic hydrogen evolution. Appl Surf Sci. 2018;462:423–431. doi:10.1016/j.apsusc.2018.08.126
61. Gogoi D, Koyani R, Golder AK, Peela NR. Enhanced photocatalytic hydrogen evolution using green carbon quantum dots modified 1-D CdS nanowires under visible light irradiation. Sol Energy. 2020;208:966–977. doi:10.1016/j.solener.2020.08.061
62. Yang C, Zhu Y, Liu Y, Wang H, Yang D. Ternary red phosphorus/CoP_2/SiO_2 microsphere boosts visible-light-driven photocatalytic hydrogen evolution from pure water splitting. J

 DOI: 10.15826/chimtech.2023.10.2.03

Mater Sci Technol. 2022;125:59–66. doi:10.1016/j.jmst.2022.02.034
63. Liu H, Chen J, Guo W, Xu Q, Min Y. A high efficiency water hydrogen production method based on CdS/WN composite photocatalytic. J Colloid Interf Sci. 2022;613:652–660. doi:10.1016/j.jcis.2022.01.014
64. Xu Z, Guo C, Liu X, Li L, Wang L, Xu H, Zhang D, Li C, Li Q, Wang W. Ag nanoparticles anchored organic/inorganic Z-scheme 3DOMM-TiO_{2-x}-based heterojunction for efficient photocatalytic and photoelectrochemical water splitting. Chin J Catal. 2022;43(5):1360–1370. doi:10.1016/S1872-2067(21)63978-5
65. Tian Z, Yang X, Chen Y, Huang H, Hu J, Wen B. Fabrication of alveolate g-C_3N_4 with nitrogen vacancies via cobalt introduction for efficient photocatalytic hydrogen evolution. Int J Hydrog Energy. 2020;45(46):24792–24806. doi:10.1016/j.ijhydene.2020.06.274
66. Ma X, Li W, Li H, Dong M, Li X, Geng L, Fan H, Li Y, Qiu H, Wang T. Fabrication of novel and noble-metal-free MoP/In_2S_3 Schottky heterojunction photocatalyst with efficient charge separation for enhanced photocatalytic H_2 evolution under visible light. J Colloid Interf Sci. 2022;617:284–292. doi:10.1016/j.jcis.2022.03.021
67. Liang Z, Yang C, Lu J, Dong X. Ultrathin Fe2P nanosheet co-catalyst CdS nanorod: The promising photocatalyst with ultrahigh photocatalytic H_2 production activity. Appl Surf Sci. 2021;566:150732. doi:10.1016/j.apsusc.2021.150732
68. Zhong Y, Yang S, Zhang S, Cai X, Gao Q, Yu X, Xu Y, Zhou X, Peng F, Fang Y. CdS branched TiO_2: Rods-on-rods nanoarrays for efficient photoelectrochemical (PEC) and self-bias photocatalytic (PC) hydrogen production. J Power Sources. 2019;430:32–42. doi:10.1016/j.jpowsour.2019.04.116
69. Boppella R, Choi CH, Moon J, Kim DH. Spatial charge separation on strongly coupled 2D-hybrid of rGO/$La_2Ti_2O_7$/NiFe-LDH heterostructures for highly efficient noble metal free photocatalytic hydrogen generation. Appl Catal B-Environ. 2018;239:178–186. doi:10.1016/j.apcatb.2018.07.063
70. Guo C, Tian K, Wang L, Liang F, Wang F, Chen D, Ning J, Zhong Y, Hu Y. Approach of fermi level and electron-trap level in cadmium sulfide nanorods via molybdenum doping with enhanced carrier separation for boosted photocatalytic hydrogen production. J Colloid Interf Sci. 2021;583:661–671. doi:10.1016/j.jcis.2020.09.093
71. Rabell GO, Cruz MRA, Juárez-Ramírez I.Photoelectrochemical (PEC) analysis of ZnO/Al photoelectrodes and its photocatalytic activity for hydrogen production. Int J Hydrog Energy. 2022;47(12): 7770–7782. doi:10.1016/j.ijhydene.2021.12.107
72. Huang K, Li C, Zhang X, Wang L, Wang W, Meng X. Self-assembly synthesis of phosphorus-doped tubular g-C_3N_4/Ti_3C_2 MXene Schottky junction for boosting photocatalytic hydrogen evolution. Green Energy Environ. 2023;8(1):233–245. doi:10.1016/j.gee.2021.03.011
73. Mahvelati-Shamsabadi T, Fattahimoghaddam H, Lee B-K, Ryu H, Jang JI. Caesium sites coordinated in Boron-doped porous and wrinkled graphitic carbon nitride nanosheets for efficient charge carrier separation and Transfer: Photocatalytic H_2 and H_2O_2 production. Chem Eng J. 2021;423:130067. doi:10.1016/j.cej.2021.130067
74. Deng Q, Ba G, Huo T, Li H, Hou W. Atomic carbon chain-linked polymeric carbon nitride: Roles of the carbon chain in enhancing the photocatalytic hydrogen evolution performance. Appl Catal A-Gen. 2020;606:117833. doi:10.1016/j.apcata.2020.117833
75. Zhao H, Fu H, Yang X, Xiong S, Han D, An X. MoS2/CdS rod-like nanocomposites as high-performance visible light photocatalyst for water splitting photocatalytic hydrogen production. Int J Hydrog Energy. 2022;47(13):8247–8260. doi:10.1016/j.ijhydene.2021.12.171
76. Li X, Hu J, Yang T, Yang X, Qu J, Li CM. Efficient photocatalytic H_2-evolution coupled with valuable furfural-production on exquisite 2D/2D $LaVO_4$/g-C_3N_4 heterostructure. Nano Energy. 2022;92:106714. doi:10.1016/j.nanoen.2021.106714
77. Sun B, Qiu P, Liang Z, Xue Y, Zhang X, Yang L, Cui H, Tian J. The fabrication of 1D/2D CdS nanorod@Ti_3C_2 MXene composites for good photocatalytic activity of hydrogen generation and ammonia synthesis. Chem Eng J. 2021;406:127177 doi:10.1016/j.cej.2020.127177
78. Zhang Q, Chen D, Song Q, Zhou C, Li D, Tian D, Jiang D. Holey defected TiO2 nanosheets with oxygen vacancies for efficient photocatalytic hydrogen production from water splitting. Brit Cer Pr. 2021;23:100979. doi:10.1016/j.surfin.2021.100979
79. Zhang K, Mou Z, Cao S, Wu S, Xu X, Li C. Well-designed NiS/CdS nanoparticles heterojunction for efficient visible-light photocatalytic H_2 evolution. Int J Hydrog Energy. 2022;47(25):12605–12614. doi:10.1016/j.ijhydene.2022.02.009
80. Attia S, Helaïli N, Bessekhouad Y, Trari M. Physical properties of the solid solution $CuFe_{2-x}Mn_xO_4$ prepared by sol-gel route: Application to photocatalytic hydrogen production. J Photoch Photobio A. 2022;426:113745. doi:10.1016/j.jphotochem.2021.113745
81. Markovskaya DV, Zhurenok AV, Kozlova EA. Rate of photocatalytic hydrogen evolution and photovoltaic characteristics as a function of the nature and concentration of the electrolyte. Rus J Phys Chem A. 2022;96(5):1093–1098. doi:10.1134/S003602442205020X

 DOI: 10.15826/chimtech.2023.10.2.03